UNIVERSITY OF OKLAHOMA

GRADUATE COLLEGE

MISSION-ORIENTED DESIGN AND OPTIMIZATION OF A HYBRID FUEL CELL-BATTERY SYSTEM FOR UNMANNED AERIAL VEHICLES

A THESIS

SUBMITTED TO THE GRADUATE FACULTY

in partial fulfillment of the requirements for the

Degree of

MASTER OF SCIENCE

By SHANNON MATHERS

Norman, Oklahoma

2026

Downloaded from SHAREOK. Persistent Handle URL: https://hdl.handle.net/11244/342574

MISSION-ORIENTED DESIGN AND OPTIMIZATION OF A HYBRID FUEL CELL-BATTERY SYSTEM FOR UNMANNED AERIAL VEHICLES

A THESIS APPROVED FOR THE

SCHOOL OF AEROSPACE AND MECHANICAL ENGINEERING

BY THE COMMITTEE CONSISTING OF

Dr. Pejman Kazempoor, Chair

Dr. Wilson Merchan Merchan

Dr. Iman Ghamarian

©Copyright by SHANNON MATHERS 2026
All Rights Reserved.

Acknowledgements

First, I would like to thank Professor Pejman Kazempoor for his support in this research and thesis writing process. His guidance and feedback helped me finish this thesis and explore fuel cell technology. I want to acknowledge his hard work as the chairperson of my committee and the time he committed to teaching me.

Thank you to my committee members, Professor Wilson Merchan-Merchan and Professor Iman Ghamarian, for taking the time to support me and my work. Their teachings and thoughtful feedback have strengthened my research and my professional growth. I also want to thank Zhicheng Xu for his extensive work helping me troubleshoot my model and Claire Lindley from the Writing Center for her hours of revision discussions and improvements.

A special thank you to Professor Dominique Pittenger, who has been a steadfast mentor since I arrived at OU six years ago. In our weekly meetings, she has reminded me all that I am capable of and to enjoy the process of research. I could not have reached the finish line without her mentorship and guidance.

To my friends, classmates, and roommate, thank you for encouraging me, listening to my research, and supporting me from early drafts to defense. It means so much that you choose to watch my thesis defense. I would like to express my sincere gratitude for my family and their support. My educational journey would not be possible without them. Mom, thank you for helping me focus through this process; Dad, thank you for nurturing my passion for engineering.

Finally, I would like to thank God for the people he blessed me with in this educational journey. He is able to do immeasurably more than I could ask or imagine, and I have seen this throughout my time at OU. I am endlessly grateful for His love and His plan for my life.

Table of Contents

Acknowledgements iv
Table of Contents v
Table of Figures vii
Table of Tables ix
Abstract x
Chapter 1: Introduction 1
1.1 What are Unmanned Aerial Vehicles? 1
1.2 What is a Propulsion System? 3
1.3 What is a Fuel Cell? 4
1.4 Purpose of Research 5
1.5 Research Objective 5
1.6 Research Question 6
1.7 Point of Departure 6
1.8 Thesis Outline 6
Chapter 2: Literature Review 8
2.1 Fuel Cell 9
2.2 Battery 12
2.3 UAV 13
2.4 Energy Management System 14
2.4.1 Propulsion 14
2.4.2 Configuration 14
2.4.3 Logic 16
2.5 Temperature and Moisture Management 18
2.5.1 Coolant 18
2.5.2 Flow Structure 18
2.5.3 Humidity Management 20
2.5.4 Environmental Factors 20
2.6 Hydrogen Storage 21
2.6.1 Main Concerns 21
2.6.2 Liquid 21

2.6.3 Solid 22
2.6.4 Gas 23
2.7 Efficiency 24
2.8 Conclusion 25
Chapter 3: Methodology 27
3.1 Software Explanation 27
3.2 Original MathWorks Model 28
3.3 Membrane Electrode Assembly 29
3.4 Gas Channels 39
3.5 Oxygen Source 41
3.6 Hydrogen Source 42
3.7 Cooling System 43
3.8 Battery Model 44
Chapter 4: Testing 53
4.1 Drive Cycle and Power 53
4.2 Fuel Cell Only Testing 54
4.3 Battery Only Testing 60
4.4 Energy Management System 63
4.5 Fuel Cell and Battery Testing 65
4.6 Parametric Study with Multiple Mission Profiles 69
4.6.1 Agriculture Mission Profile 71
4.6.2 Package Delivery Mission Profile 73
4.6.3 Surveillance Mission Profile 75
4.6.4 Discussion of Results 77
Chapter 5: Summary and Future Work 79
5.1 Summary 79
5.2 Future Work Recommendations 80
References 83

Table of Figures

Figure 1 A summary of different UAV applications across industries 2
Figure 2 A diagram of UAV categories and visual examples of each type (Adoni et al., 2023)..... 3
Figure 3 A diagram of a PEMFC, detailing the electricity generation through the electrochemical reaction (MathWorks, n.d.) 4
Figure 4 Model of a PEMFC (Samosir et al., 2010) 10
Figure 5 Rule-based Energy Management Strategy (Xiao et al., 2023) 17
Figure 6 Flow channels of different models within fuel cell (Toghyani et al., 2021)..... 19
Figure 7 Temperature distribution in Kelvin of multiple flow channels (Toghyani et al., 2021) . 20
Figure 8 The overall Simulink and Simscape model of a PEM Fuel Cell System (Mathworks, 2025) 29
Figure 9 The user-defined default parameters in the MATLAB source code within the MEA Simscape block (Mathworks, 2025) 30
Figure 10 The internal parameters in the MATLAB source code within the MEA Simscape block (Mathworks, 2025)..... 31
Figure 11 The cathode gas channels subsystem (MathWorks, 2025) 40
Figure 12 The oxygen source subsystem (Mathworks, 2025) 42
Figure 13 The hydrogen source subsystem (Mathworks, 2025)..... 43
Figure 14 The cooling subsystem (Mathworks, 2025) 44
Figure 15 Battery Cell Model 46
Figure 16 Battery Pack Model 47
Figure 17 A Battery Pack Block in Simulink after exporting from the Simulink Battery Builder app..... 49
Figure 18 Full model with 2 battery cells 50
Figure 19 Full model with battery pack integrated..... 51
Figure 20 Example data from a simulation that fails at 2573.166 s 56
Figure 21 Fuel cell efficiency data prior to failure at 2573.166 s..... 57
Figure 22 Data from a fuel-cell-only run (battery commented out) using 400 cells in the stack for 7200 s, or 2 h..... 58
Figure 23 Fuel cell efficiency data from a fuel-cell-only run (battery commented out) using 400 cells in the stack for 7200 s, or 2 h 59
Figure 25 The battery and drive cycle, or power load, model 61
Figure 26 Data from a battery only run for 7200 s 63
Figure 27 Function blocks model with mask on drive cycle removed, see the original block commented out, which froze at 129 s 64
Figure 28 Model used for hybrid testing with systems connected by wires..... 66
Figure 29 Fuel cell scope of hybrid run for 7200 s and 400 cells in the stack 67
Figure 30 Efficiency from hybrid run for 7200 s with 400 cells in stack..... 67
Figure 31 Battery scope of hybrid run for 7200 s and 400 cells in the stack..... 68
Figure 32 The three mission profiles based on real-world UAV applications 71
Figure 33 Fuel cell scope of agriculture mission..... 72

Figure 34 Fuel cell efficiency of agriculture mission 72
Figure 35 Battery scope of agriculture mission 73
Figure 36 Fuel cell scope for delivery mission 74
Figure 37 Fuel cell efficiency for delivery mission 74
Figure 38 Battery scope for delivery mission 75
Figure 39 Fuel cell scope for surveillance mission 76
Figure 40 Fuel cell efficiency for surveillance mission 76
Figure 41 Battery scope for surveillance mission 77

Table of Tables

Table 1 Model Equations 32
Table 2 Mission Phase Times (s) 69

Abstract

As unmanned aerial vehicles (UAVs) become increasingly integral to sectors such as agriculture, defense, and emergency healthcare, the need for more flexible power sources also increases. Relying solely on one method of propulsion limits the capability of UAVs. A hybrid propulsion system can implement multiple power sources to better address specific mission needs. This thesis details the mission-oriented design and optimization of a hybrid propulsion system combining a Proton Exchange Membrane Fuel Cell (PEMFC) and a lithium-ion battery for a fixed-wing UAV.

The research utilizes MATLAB, Simulink, and Simscape platforms to develop a high-fidelity digital representation of the hybrid power system. In addition, the research integrates a detailed PEMFC 400-cell stack with a battery pack circuit. The performance of this hybrid model is evaluated through a parametric study involving three distinct mission profiles: agriculture, package delivery, and surveillance.

The results demonstrate that the hybrid configuration leverages the high energy density of the fuel cell for sustained cruise flight while utilizing the battery's superior power density to meet rapid demand spikes during takeoff and climbing. Overall, the hybrid system provides approximately twenty percent higher thermal efficiency and reduced mechanical strain compared to individual power sources. While the current model is best suited for missions lasting between 1 and 1.5 hours, this study provides a framework for future work, emphasizing the potential for energy management systems and more powerful batteries to further extend flight endurance and mission capabilities.

Chapter 1: Introduction

This section introduces unmanned aerial vehicles and their propulsion systems across various applications. In this chapter, both engineering challenges and current literature support are discussed. Fuel cells are explained and defined as a key propulsion method alongside batteries. The purpose of research and potential of hybrid systems are discussed in relation to the mission profile and flight goals. The research objective describes the methods of research and tools, and the research questions to be answered are listed as well.

1.1 What are Unmanned Aerial Vehicles?

Unmanned aerial vehicles (UAVs) are flying objects that can be controlled remotely or fly autonomously. They come in a range of sizes and fly at altitudes that span from just above the ground into orbits. The technology and prevalence of UAV development are both relatively new. While the military has been building UAVs for surveillance since the twentieth century, the Federal Aviation Administration allowed UAVs in civilian airspaces in 2006. From there, the market rapidly expanded with many applications of the technology. Defense continues to invest in UAVs for conventional weapons, surveillance, border control, crime control, and applications in space (Kapoor et al., 2023). In agriculture, UAVs can monitor irrigation, livestock, crops, and weeds to improve farming efficiency (Adoni et al., 2023). Firefighters use UAVs equipped with infrared sensors to evaluate fire size at an aerial view and detect hotspots. In healthcare, researchers are simulating and testing UAVs to deliver medications and defibrillators to remote or disaster-impacted areas faster than ambulances could reach patients (Hussain et al., 2024). UAVs will impact national security, food production, and lifesaving technology for future

generations. Today, UAVs are also used by the public in delivery, search and rescue missions, photography, racing, and recreation. Each application has different priorities, ranging from speed, payload capacity, flight time, or stealth (Figure 1).



Figure 1 A summary of different UAV applications across industries

UAVs can be categorized based on size, geometry, and power sources, to name a few. The wingspan and weight can each be metrics to determine a UAV's category. Below in Figure 2 are some photos of various UAVs to illustrate the range of designs. Some fly in a quad copter style, using vertical lift as takeoff mechanism. There are also fixed wing models that more closely resemble planes and takeoff after taxi. The amount and type of power are also categories. Power is provided by a propulsion system, and different types of propulsion systems are suited to different applications. Each system has weaknesses when analyzed independently, and studying the combination and optimization of systems can overcome some of these limitations.

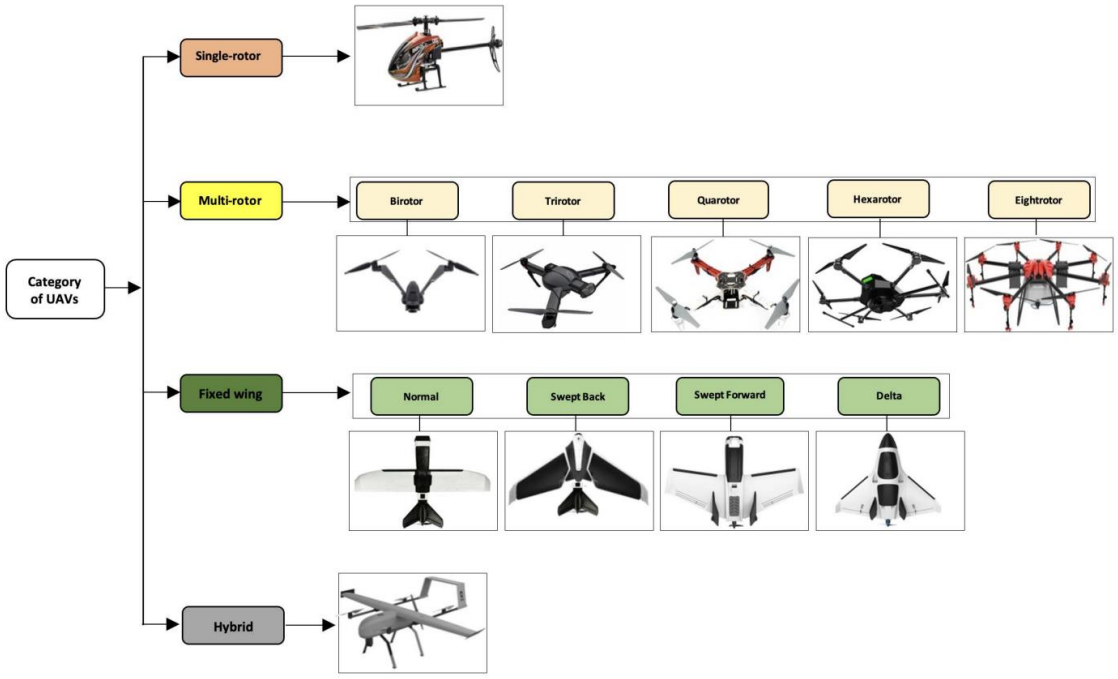

Figure 2 A diagram of UAV categories and visual examples of each type (Adoni et al., 2023)

1.2 What is a Propulsion System?

A propulsion system provides power and enables UAV flight. The choice in a UAV's propulsion method is dependent on its mission and flight profile. Just like a car can run on different fuels or be a hybrid system, UAVs have many options and combinations of power. Internal combustion engines, batteries, fuel cells, and solar power are all possibilities for UAV power, and a hybrid system can use a combination of the above methods. Within each of these categories, further subcategories exist. For instance, the type of cycle running in the combustion engine could be Otto, Rankine, or Carnot. Likewise, the chemical within a fuel cell and temperature operation varies based on selection. The fuel cell substance is hydrogen for a proton exchange membrane fuel cell (PEMFC), whereas methanol powers a direct methanol fuel cell (DMFC). Each propulsion system has strengths and tradeoffs, and the mission profile and environment influence the choice of propulsion system to achieve the best outcomes.

1.3 What is a Fuel Cell?

A fuel cell is an electrochemical system that is highly energy dense. Hydrogen fuel cells use hydrogen and oxygen to produce fuel and water as a byproduct in a process called electrolysis. Other fuel cells can be powered by methanol, phosphoric acid, or solid oxides. A PEMFC is a proton exchange membrane fuel cell, and it is a type of hydrogen fuel cell. It operates at lower temperatures of 20 to 100 degrees Celsius, whereas other fuel cells operate at much higher temperatures, such as solid oxide fuel cells, which can reach up to 1,000 degrees Celsius. A PEMFC is predicted to work best for missions where avoiding heat detection is important, and it is a commonly used fuel cell. The Department of Energy continues to invest in research and development in fuel cell and hydrogen technology for a variety of applications, including airborne systems. A diagram of a PEMFC is shown below in Figure 3.

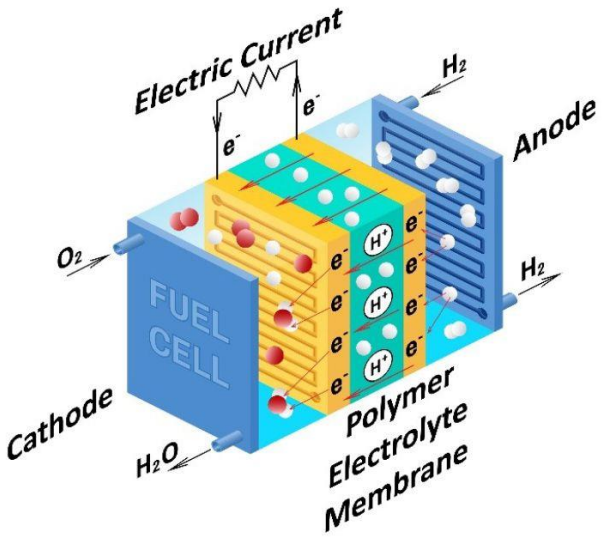

Figure 3 A diagram of a PEMFC, detailing the electricity generation through the electrochemical reaction (MathWorks, n.d.)

1.4 Purpose of Research

Internal combustion engines are loud and very easy to detect on a heat seeker. Fuel cells have low power density and cannot provide a large amount of power with a quick demand. Fuel cells are good for endurance, efficiency, lower emissions, and stealth. Batteries can provide power on demand and have a high power density, which fuel cells struggle to achieve. Thus, a hybrid system can combine benefits of each propulsion system and avoid disadvantages of relying solely on one method. UAVs in the defense industry face unique challenges with high altitude flight in surveillance, a need for stealth and lack of heat in reconnaissance, and overall range for longer missions than typical commercial UAVs. This computational research investigates a system using a PEMFC, a lithium-ion battery, and a fixed-wing UAV.

1.5 Research Objective

The simulations in this thesis use a hybrid model of UAV to leverage advantages of separate propulsion methods. In the simulations, the program follows a defined flight profile and mission, along with the appropriate parameters of external factors, mass of UAV, and type of equipment. The project simulates and model the system in Matlab Simulink that corresponds to the mission. After initial simulations, focus shifts to optimization. This can include improvement of settings to manage energy most efficiently between the battery and fuel cell to achieve longer ranges, higher altitude paths, and increased flight time.

1.6 Research Question

The research presented in this paper aims to answer questions regarding system operations, mission achievements, and optimization. How is the system impacted with a hybrid operation? Are there multiple missions or applications this UAV can achieve? How do altitude, oxygen pressure, temperature, and humidity impact a UAV powered by a PEMFC and battery hybrid propulsion system within a MATLAB and Simulink environment? These questions seek to improve the system and use technology to study optimization efforts.

1.7 Point of Departure

Hybrid models of UAVs are widely accepted as a solution to the power density struggles of fuel cells and energy density shortfalls of batteries. Previous research also simulates UAV flight with a defined mission profile. With the described research on hybrid fuel cell battery UAVs, the goal of this study is to simulate different conditions than found in literature, especially when facing different environments. Previous literature has used MATLAB and Simulink models to simulate a PEMFC-powered UAV at one defined mission profile (Corcau, 2025). The research in this thesis also uses a MATLAB and Simulink model of a UAV, and it analyzes the system by changing parameters including number of fuel cells, mission type, and power demand.

1.8 Thesis Outline

The following is an outline for the remainder of the thesis. In chapter one, an introduction to the topic of fuel cell UAVs and the research goals regarding mission-oriented design and optimization is provided. In chapter two, a review of the current literature and studies in

simulations, design, and flight tests of UAVs powered by fuel cells and the evolution of fuel cells in power is detailed, all research which helped inform the topic and departure from the literature. Chapter three details the methodology of this thesis through simulations in MATLAB and Simulink. This includes programs, functions, method of creating a controls model and testing the system, and all related parameters and their origins. Chapter four analyzes the results of the simulations and their implications for the range and power of the UAV system in relation to the mission and flight profile. Finally, chapter five concludes the thesis with key takeaways and potential future work, such as continual optimization.

Chapter 2: Literature Review

Hydrogen fuel cells come in many forms, and each has a varying internal structure, fuel composition, storage method, and applications. The Proton Exchange Membrane Fuel Cell (PEMFC) is viewed as a reliable option for unmanned aerial vehicle (UAV) applications. Some factors contributing to its benefits include a low operating temperature below 100° C, a high energy or power density, and an aptitude for endurance missions, especially with the fuel cell's ability to meet power demand and sustain cruise flight for long periods of time.

The advantages of fuel cells over internal combustion engines include environmental benefits of mitigating CO_2 emissions and the renewable nature of the fuel cell cycle in its reactions. However, fuel cells provide mission-specific benefits alongside sustainable energy motivations. In military and defense applications, a fuel cell can be more effective than an internal combustion engine through a lower noise level and less heat produced, which can enhance the stealth capabilities of a UAV in reconnaissance and other defense-related applications.

This literature review finds existing knowledge studying fuel cells' incorporation within UAVs as a power source and aim to further this knowledge through questions, challenges, and research opportunities by examining the different components in a hybrid hydrogen fuel cell and battery powered UAV system. The subsections cover options within the component, current practices in UAV testing and modeling, and scientific principles or measurements behind each component. Alongside the process and design of the component, this study presents challenges associated with each part and explores novel research methods of addressing challenges as applicable. Improvements in each component ultimately lead to a cost-effective, efficient, and mission-capable system mitigating risks to human pilots and advancing stealth technologies.

2.1 Fuel Cell

A fuel cell relies on electrochemical reactions to produce fuel. Electrochemical reactions convert chemical energy into electrical energy without combustion methods of other fuels. Fuel cells also have fewer moving parts than other motors, a benefit for longevity and maintenance. One promising fuel cell option is a proton exchange membrane fuel cell (PEMFC), with a model shown in Figure 4 below. Other names include proton electrolyte membrane or polymer electrolyte membrane. In these models, a cathode and an anode facilitate electrochemical reactions for fuel.

The membrane electrode assembly (MEA) is a critical component of the fuel cell. The MEA houses the proton exchange membrane (PEM) which allows the passing of protons through the membrane while blocking the passing of electrons. Instead, the electrons travel through an external circuit and generate electrical power (Samosir et al., 2010). This electron barrier is also called an electrolyte, as seen in one of the names of the fuel cell. The passing of protons and exchange of electrons with ions is why the name uses exchange to show the transfer of ions between the reactants and the products in an electrochemical reaction.

The PEM is made of a fluoropolymer material that conducts protons, often Nafion, which is why polymer electrolyte membrane is also a name for the fuel cell (Wang et al., 2020). On each side of the PEM is a metal catalyst layer to facilitate the electrochemical reactions within the fuel cell. Often, the catalyst is one of the most expensive parts of the fuel cell. The catalyst is usually platinum or another type of noble metal. Materials scientists are exploring new possibilities for affordable catalysts, and one fuel-cell powered UAV incorporated a cobalt catalyst in its design (Pan et al., 2019). Hydrogen is split into hydrogen ions and electrons in the anode, with electrons passing through an external circuit to generate power. The ions move

across the catalyst layers and membrane to the cathode and combine with electrons and oxygen to form water as a product. “An oxidizer and a fuel react to form [water]. The fuel is typically hydrogen, and the oxidizer is usually the oxygen from air. The oxygen (air) continuously passes over the cathode and the hydrogen passes over the anode to generate electricity, by-product heat and water” (Samosir et al., 2010). The production of water in fuel cells and ranges of fuel cell operation in temperature and humidity are addressed with dehumidification processes in the system and other considerations in engineering to address environmental concerns.

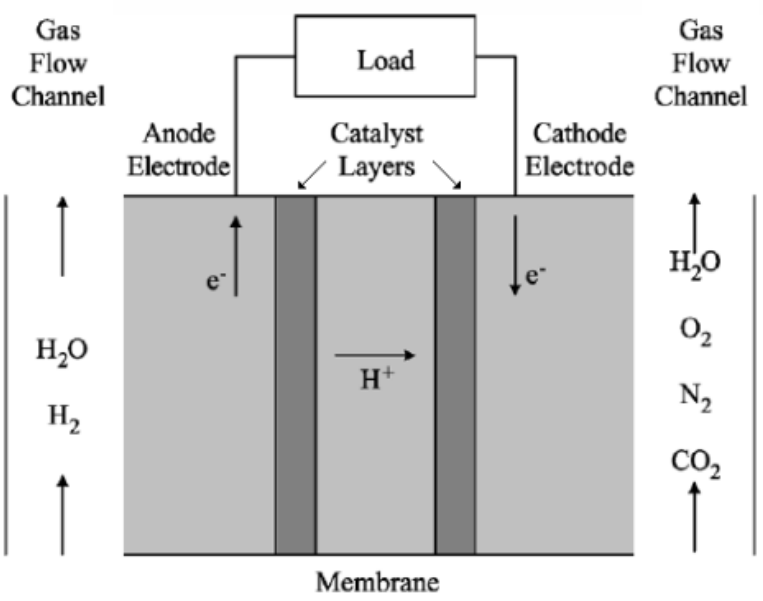

Figure 4 Model of a PEMFC (Samosir et al., 2010)

It takes more than one fuel cell to power a UAV; multiple fuel cells are organized in stacks to generate enough energy to power flight. Bipolar plates (BPs) serve as a connection between each fuel cell and can allow fuel cell stacks to achieve higher voltages and more power. However, each component of the system contributes to the weight, an important factor to consider in flight applications. BPs account for “60–80% of the fuel cell weight and 30–50% of the stack manufacturing cost [12]. For this purpose, the fuel cell stack’s weight and cost can be

significantly reduced by improving BP configuration and the embedded flow field within BPs and using lightweight material" (Toghyani et al., 2021). The continuing research of fuel cells incorporates weight reduction, efficiency improvements, and use of new materials to reduce costs of fuel cell and UAV operation.

The electrochemical reaction in a PEMFC has different factors to analyze as well, spanning disciplines of engineering. The open circuit voltage within a fuel cell is affected by the fluid flow, pressure, and humidity in the system. Frequency can be measured based on the reaction rates of electrodes and transport of ions across the membrane. Thermodynamics are also crucial in determining the optimal operating temperature and managing the system in extreme temperature situations, as well as pressure challenges of storing hydrogen for the reactions (Lee & Cho, 2009).

PEMFCs are uniquely well-suited to UAV applications due to low temperature operation range and high energy density. Energy density is the amount of energy that can be produced per unit of mass of the system. A high energy density allows for an increase in mission range and less frequent stops for refueling. With fuel cells continuing to refine systems and incorporate within UAVs, especially in conjunction with other power sources as a hybrid system, aircraft can fly continuously without fuel limitations or relying on a human pilot. In addition to low operating temperatures, PEMFCs have "solid phase electrolyte and the ability to operate with CO_2 in the air stream which makes them the most appropriate type of fuel cell for use in aerial vehicles" (Gadalla & Zafar, 2016). Most of the fuel cell UAV research focuses on the PEMFC as the optimal choice for power, and it has performed well in modeling and flight tests.

Fuel cells can be enhanced by using a hybrid system, for instance a fuel cell with a battery, to accommodate different power loadings in flight phases. For cruise, fuel cells are

effective at maintaining a constant power output and can charge the battery during this phase as well. For more power-intensive phases of flight, such as takeoff, a battery is a practical way to meet high power demands quickly rather than forcing the fuel cell to meet starkly different power levels over time. Other hybrid options include photovoltaic sensors or solar powered cells, supercapacitors, and even internal combustion engines.

2.2 Battery

UAVs that use hydrogen fuel cells can also incorporate a battery propulsion system to create a hybrid power system. The most important factors of the battery are its power density, weight, and type, as these will impact the flight endurance and longevity of the UAV. The size of the battery pack is another variable which will "critically influence the overall power system's performance and weight" (Mariscal et al., 2024). Specific power measures the power output relative to units of mass and is measured in W/kg, whereas power density measures power output per unit of volume. Both measurements are relevant to minimize mass and space of the battery on the UAV while still delivering sufficient power for demanding scenarios, such as takeoff. The battery should be selected based on "the amount of energy required for conditioning the fuel cell [in watt-hours] and… the amount of energy that will be required for the use of the battery in the power requirement of the aircraft exceeding the capacity of the fuel cell" (Ozbek et al., 2021).

Lithium-ion batteries have advantages over other battery types due to "their higher specific power, longer cycle life, and lower self-discharge property" (Pan et al., 2019). Due to high energy densities, "Lithium-ion or lithium-polymer batteries are suitable… compared to other types of batteries. In lithium-based batteries, the charging time does not increase with increasing current" (Farajollahi et al., 2022). Lithium-ion batteries have other advantages, including their "charge for decent time and [ability to] stay charged in storage. They are lighter

than other types of batteries for same capacity. Li-ion battery chemistry delivers a high open-circuit voltage. Also, they have low self-discharge rate and reduced toxicity" (Bayrak et al., 2020).

Within the different types of lithium batteries, it is best to choose one with "relatively high power density around 500~2800 W/kg" to address high-frequency and pulsed power demand (Wang et al., 2020). Lithium batteries should be examined for performance, as deep discharge operations can degrade a battery over time, as seen in decreases in output voltage and reduced capacity (Xiao et al., 2023). Within lithium-ion batteries, nickel manganese cobalt (NMC) and lithium titanite oxide (LTO) batteries are most efficient, and "LTO enjoys the highest performance, lifespan, and safety at higher cost, whereas NMC provides acceptable performance with low cost and high specific energy" (Pourrahmani et al., 2022). For initial testing of the UAV, NMC batteries can effectively power the UAV in a hybrid configuration with the fuel cell while managing overall costs of the system, as seen in the study selecting NMC batteries for analysis. In the future, lithium-air batteries have the potential to significantly increase energy density compared to existing lithium batteries, but these models are not yet commercially available (Depcik et al., 2020). Continuous improvement in battery packs will further support fuel cell power and its flight applications with more energy within less mass.

2.3 UAV

The integration of a fuel cell within a UAV requires a purposeful UAV design and flight constraints within the capacity of the power system. Fixed-wing UAVs are the most developed and best suited to outdoor missions at high speeds of 6-20 m/s, which aligns with defense applications of surveillance (Pan et al., 2019). When a UAV climbs, it should only use power up to the peak-power of the battery and fuel cell, otherwise the battery longevity is compromised

(Wang et al., 2020). Besides the power limitations and speed consideration, the flight mechanics of the UAV are essential. The placement of fuel cell stacks, battery packs, and other equipment shifts the center of gravity, adds weight, and impacts drag. Another flight design variable is static margin: “the difference between the distance from the leading edge of the wing to the neutral point minus the distance from the leading edge to the aerodynamic center of the aircraft” which provides stability to the UAV at a positive value (Herwerth et al., 2006). Positive static margin and stability protect the fuel cell, hydrogen tanks, and UAV from a tendency to pitch. The airfoil and lift generation are also important design considerations for successful flight, and the UAV depends on its construction and aerodynamics in conjunction with propulsion methods.

2.4 Energy Management System

2.4.1 Propulsion

The propulsion system of a UAV determines where the UAV will draw power and how much power it can use while maintaining an acceptable weight for flight. There are a variety of power sources, including internal combustion engines, photovoltaic cells, supercapacitors, batteries, and hydrogen fuel cells. The propulsion system has the greatest impact on the “flight endurance, specific energy, and specific power” of the UAV (Pan et al., 2019). The most straightforward approach may be to choose one system, but hybrid options, which incorporate more than one type of propulsion, are growing in effectiveness. Because “pure fuel cell power propulsion system is the simplest, but it cannot adapt to various load requirements” adopting a hybrid strategy is often a better choice for longevity and power (Xu et al. 2022).

2.4.2 Configuration

An energy management system (EMS) is essential to productively allocate power from each propulsion source to the UAV. The EMS accomplishes this goal while also supplying

enough power to safely satisfy the flight requirements. An EMS also keeps the power sources in the best possible condition while avoiding burnout or long-term limitations due to high strain on power sources (Xu et al. 2022). The battery not only supplies additional power to meet demand, but also meets quickly changing demands in a way that a fuel cell cannot quickly adapt to, such as takeoff or climbing scenarios (Santos et al., 2022). Since "fuel cells have high energy density but low power density," the power density of a battery is complementary to the fuel cell in UAVs (Kim et al., 2011). If a hybrid system were not used, the fuel cell system required to generate the same amount of power would be larger and more costly than hybrid options (Gadalla & Zafar, 2016). The hybrid system alleviates the fuel cell from having to adjust to large changes in output, and "frequent fluctuations in PEMFC output power would cause a rapid change in the internal electrochemical reaction rate, which may lead to irreversible damage to the internal bipolar plates and proton exchange membrane of the PEMFC" (Xiao et al., 2023). Even with an EMS, the changing fuel cell power levels will erode the function and longevity of the fuel cell, but not as substantially as drastic changes in the absence of a hybrid system.

The electrical configuration of the power sources determines the amount of control and potential risks of harm from excessive current or substantial voltage differences. A hybrid system can be direct or indirect. With a direct hybrid construction, there is no converter, and the fuel cell and battery are connected. However, there is a risk with differing voltage outputs in the battery and fuel cell that the back current may damage the fuel cell (Wang et al., 2020). The direct hybrid configuration cannot control the individual power sources as well as an indirect method.

An indirect hybrid system allows for more control over which propulsion device provides power in different situations, but it requires an energy management system, often in the form of a microcontroller or DC-DC converter. An indirect system can be semi-active or fully-active, but a

fully-active system usually requires two DC-DC converters to control the energy management, which adds a substantial amount of weight to the system (Wang et al., 2020). For this reason, a semi-active solution may be optimal. Depending on the difficulty of replication, Xiao introduced a novel EMS where "in comparison with the conventional fully-active construction utilizing two DC-DC converters, the proposed fully-active PEMFC-Lithium battery hybrid power system holds advantages in simplicity, weight, size and efficiency, achieving fully-active control of the PEMFC and the Lithium battery using only one DC-DC converter" (Xiao et al., 2023). This is a substantial advancement in the control of propulsion and power sources while considering the challenges of weight and space on a UAV.

2.4.3 Logic

In addition to the electrical circuit connecting the power sources, the EMS must know when to use which power source, detect when the UAV is experiencing a high power demand, and charge or discharge the battery at optimal voltage levels and time. The battery charging often happens during cruise flight when the fuel cell is exerting most of the power at a constant rate. The differences between battery and fuel cell voltages are reduced as the battery is charged, and the fuel cell output and charging rate decrease with a charged battery (Kim et al., 2011). This prevents overcharging or damaging the battery and allows the voltages between two systems to equalize. A logical sequence of questions and power output can determine when the EMS switches between systems. One method is rule-based strategy, incorporating a flow chart of rigid numerical values to arrive at the answer of which power source to use (see Figure 5). This method sets the initial parameters of the flow chart and does not require training of a dataset as a neural network or categorizing ranges as fuzzy logic, providing a simple way to control the power switch. An example of this is shown in Xiao's study (2023).

Another example EMS is fuzzy logic, which assigns each variable a level based on the ranges predetermined by earlier experiments and uses low, medium, or high indicators to make decisions (Wang et al., 2020). This method is attributed more closely to human intelligence based on its ability to operate with ranges and less methodically than a rule-based strategy. A third method, which will likely see growing popularity in the future, are neural networks. The neural networks are most closely connected with artificial intelligence and can improve energy consumption by adjusting existing frameworks of fuzzy logic or other strategies (Wang et al., 2020). Managing logic and electrical components requires understanding of algorithms, programming the system, and a complex chain of sensors to decide on the best power distribution throughout flight.

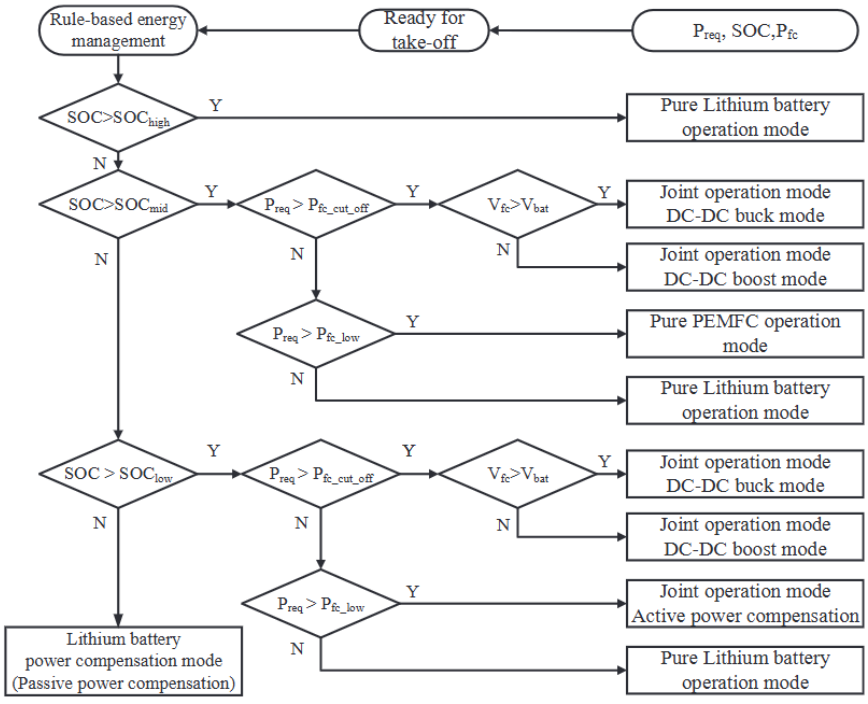

Fig. 9. Rule-based energy management strategy.

Figure 5 Rule-based Energy Management Strategy (Xiao et al., 2023)

2.5 Temperature and Moisture Management

2.5.1 Coolant

The temperature of a fuel cell is also crucial to operation efficiency. PEMFCs can run in a temperature range of 30-100° C, but "excess temperature can lead to membrane dehydration, decreasing proton mobility" (Santos et al., 2022). The highest power output of a fuel cell happens in 50-70° C, but heating the fuel cell in cold temperatures can take time, and maintaining the temperature in the optimal or acceptable range can be a challenge (Wang et al., 2020). Fuel cells use coolant to keep temperatures down, either in liquid or gas form. Liquid coolant requires more power, as it is denser than a gas coolant. Using air as a coolant is a better choice for UAVs to minimize the weight and power required for the system, but research continues to work towards improving the power density of gas coolant to the levels of liquid coolant (Toghyani et al., 2021).

2.5.2 Flow Structure

The structure within a fuel cell can also impact temperature and the heat management of the flow of reactants and products. Parallel channel structures are some of the most widely used, yet research exploring other structures observed better temperature management throughout the fuel cell with a bean-shaped channel. "Lower temperature views are seen in bean-shaped models than the parallel design… because the convection heat transfer coefficient raises as velocity increases, and the heat transfer in the pin vicinity improves" (Toghyani et al., 2021). The model of the flow channels is shown in Figure 6 below. The flow channel structure is a temperature management strategy separate from the coolants mentioned above, relying on the geometry of the channel to distribute heat evenly. Ultimately, the "unblocked bean-type has the best performance in terms of temperature distribution and mass power density. This novel flow

pattern is suggested for aerial applications that aim to reduce weight and attain optimal heat management" (Toghyani et al., 2021). Figure 7 below shows the heat distribution in a parallel flow compared to an unblocked-bean flow. This strategy is not possible in all UAVs, especially in studies focusing on UAV design with a commercially available fuel cell using parallel flow. However, the opportunity to cool the fuel cell within the flow channel can reduce the demand on the cooling system and ensure fuel cell longevity through safe operating temperatures.

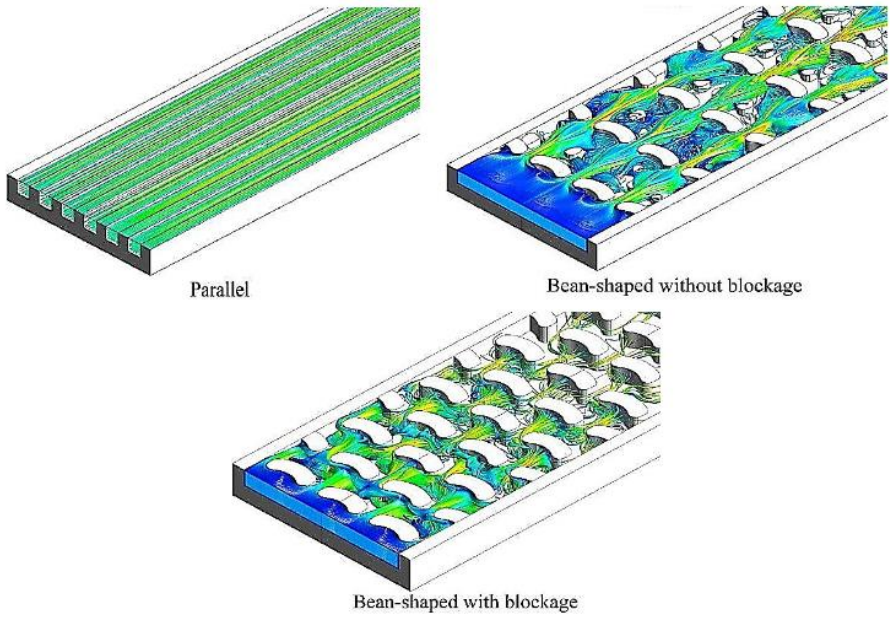

Figure 6 Flow channels of different models within fuel cell (Toghyani et al., 2021)

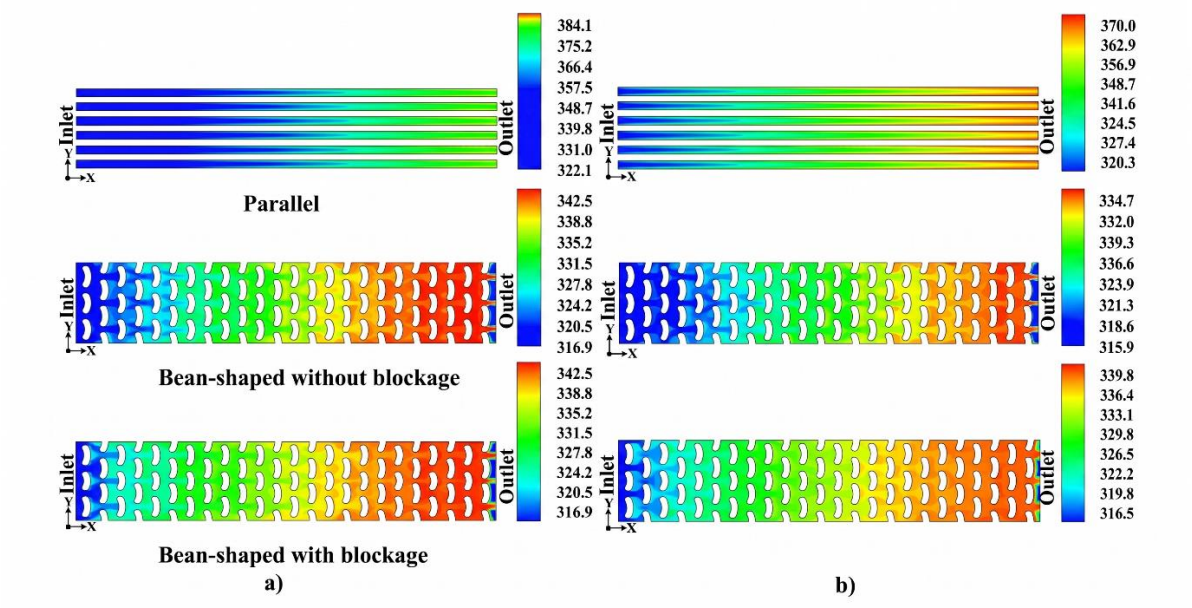

Figure 7 Temperature distribution in Kelvin of multiple flow channels (Toghyani et al., 2021)

2.5.3 Humidity Management

The reaction within a fuel cell leaves water as a product, and the humidity levels and excess liquid can be a hindrance to the fuel cell performance. The system incorporates water management and purging techniques to keep the relative humidity in an acceptable range. One way to drain excess water is through a solenoid valve purging the anode channel on a scheduled time interval (Kim et al., 2011). Humidification systems in fuel cells are also necessary, as "a low relative humidity of the atmosphere leads to a low water activity in the cathode, thus resulting in weak proton conductivity and additional ohmic losses" (Wang et al., 2020).

2.5.4 Environmental Factors

The environment greatly affects fuel cell performance in temperature, humidity, and altitude. "In high ambient temperature, the additional energy consumption will increase, because a motor fan is used to cool the FC" (Wang et al., 2020). However, in the cold, "Both the fuel and

the FC stack should be heated with extra/additional energy input, which reduces the energy efficiency" (Wang et al., 2020). Besides the temperature, the pressure can impact the ability to store hydrogen in tanks. "When the external pressure is significantly low or the ambient temperature is high, the storage capacity of hydrogen can be reduced. The inner and outer vessel design should be reconsidered for these special applications with extremely low pressure and high temperature" (Wang et al., 2020). Operation at high altitude can slow electrochemical reactions because "less oxygen could be obtained when compared with that at the low altitude, which would cause an oxygen starvation issue for the FC" (Wang et al., 2020).

2.6 Hydrogen Storage

2.6.1 Main Concerns

To fuel the electrochemical reactions of a fuel cell, hydrogen must be stored on board the UAV. This can be done through storage tanks of hydrogen gas, liquid hydrogen, or solid chemical hydrides. While gaseous storage consumes the most mass and volume of the storage types, it does not require hydrogen extraction or additional equipment. Liquid and solid storage methods can reduce the mass and volume of the storage system tanks, but at a cost of adding additional machines to reform hydrogen and specific temperature requirements. The hydrogen storage capacity on board the UAV is crucial in determining flight endurance due to fuel limitations, and the weight of the system is also a factor in mission length.

2.6.2 Liquid

Liquid hydrogen storage addresses the problem of reducing mass and volume of the vessels, but this reduction and special storage method can only be achieved through low temperatures and risks hydrogen fuel losses if this temperature is not maintained. "Storing hydrogen in its liquid phase will considerably reduce the required storage volume" yet must

remain at a low cryogenic temperature (Wang et al., 2020). Warmer temperatures cause evaporation of liquid hydrogen and thus fuel loss (Wang et al., 2020). Liquid storage of hydrocarbons such as methanol, kerosene, gasoline, or diesel can also produce hydrogen and operate with a smaller tank (Dudek et al., 2013). However, liquid storage of hydrocarbons needs thermal reactors, steam reformers, and control systems to reform the hydrocarbons into usable fuel (Dudek et al., 2013). The reforming process includes losses of hydrogen and efficiency (Dudek et al., 2013). The low temperature, production, and losses within this storage method present unique challenges that make this method best for specific requirements of low-pressure storage and compact tanks, but not for overall use.

2.6.3 Solid

Solid storage of hydrogen by itself requires extremely low temperatures, but hydrogen compounds can be stored without these requirements. These compounds, called hydrides, are chemical compounds of hydrogen and other elements. There are different types of hydrides depending on the element hydrogen reacts with, each with unique structures and chemical properties, and "the selection of each hydride for fast hydrogen production, besides the criterion for large hydrogen storage capacity, depends on the reaction limitations and the formation of the reaction products" (Khzouz et al., 2020). Storing hydrides on a UAV with equipment to reform the hydrogen from the hydride as fuel is one way to increase density of hydrogen storage. Solid chemical hydrides like sodium borohydride ($NaBH_4$) can store hydrogen at high density without cryogenic temperature, but these methods need extensive extraction equipment to produce hydrogen from solid chemical hydrides (Wang et al., 2020). The extra step of generation of hydrogen from $NaBH_4$ can also cause delays and slow response time of the fuel cell (Wang et al., 2020). While "compressed hydrogen and metal hydrides… are too bulky and heavy to satisfy the

required energy density," sodium borohydride has a high energy density, and its "alkaline solution has additional advantages: stable, nonflammable, non-toxic, and high hydrogen capacity" with a catalytic hydrolysis reaction generating hydrogen (Kim et al., 2011). This area of research shows the most promise for the future in testing a variety of compounds and manipulating hydrides to create more capacity for stable storage, but currently still faces challenges of hydrogen reform and additional equipment weight and space costs that mitigate the benefit of reducing hydrogen storage volume.

2.6.4 Gas

The simplicity of storing hydrogen gas in pressure vessels is contrasted with a large volume and mass of the tanks. Although "the mass of hydrogen fuel is typically small compared to the entire fuel cell system… the mass, volume, and cost of hydrogen storage significantly increase the mass and cost of the hydrogen-fueled PEMFCs" and can take up as much as 1/3 of the total mass (Mariscal et al., 2024). Despite the high specific energy and low mass of hydrogen gas, "the hydrogen tank contributes significantly to the system's overall mass, and the fuel cell mass only accounts for 54.9 % of the PEMFC system" (Mariscal et al., 2024). The gas storage does offer benefits, such as avoiding the need to install other equipment to reform hydrogen or efficiency losses due to extraction of hydrogen, as seen in a compressed hydrogen storage vessel providing high-purity hydrogen (Xiao et al., 2023). Another gas storage method is a metal hydride tank. The metal tank material is titanium ferrite, and the tank weight is comparable to the fuel cell system weight (Herwerth et al., 2006). While the added weight to the UAV is a disadvantage, metal hydride tanks operate at relatively low pressures, which is a safety benefit (Herwerth et al., 2006). The metal hydride tank avoids the risks associated with high pressure cylinders storing hydrogen gas. Due to availability and low cost, gas storage may be the best

entry-level solution, but novel research in hydrogen management is studying compounds to maximize efficiency in solid hydride fuel while minimizing equipment space, such as the proposal of "a volume exchange fuel tank to integrate the $NaBH_4$ solution tank and the $NaBO_2$ solution tank, leading to the minimization of the volume of the fuel cell system" (Pan et al., 2019). The hydrogen storage method directly impacts the flight endurance, and its future research may lengthen missions and lighten systems considerably.

2.7 Efficiency

The efficiency of electrochemical reactions in hydrogen fuel cells is a key factor in the increasing research and applications of the technology. Within the process itself, the reaction produces electrical energy and water, avoiding harmful products or waste materials. The fuel cell also excels in energy density, the amount of energy that can be stored per mass unit. "Fuel cells (FC) as power source for electric propulsion of UAVs show growing applications because of their energy densities that exceed 800Wh/kg in comparison to 150Wh/kg for advanced batteries. Hence, FC system weights are ca. 3.5 times less than a Li-ion battery with similar parameters" (Dudek et al., 2013). Batteries are a necessary power source for quick responses to high power demands in flight, but fuel cells can provide sustained power through compact energy. "The power density has a decisive influence on maximum speed, load capacity, altitude of flight and rate of climbing whereas energy density impacts time (range) of flight covered without the need to refuel or recharge the energy accumulator" (Dudek et al., 2013). The fuel cell directly supports flight endurance, or time of flight, to complete long-range missions.

In addition to the efficiency and energy density inherent in hydrogen fuel cells, research continues to push the boundaries of fuel cell performance. One study measured activation polarization potential in a fuel cell, a factor in electrical losses in the circuit, and found that

“increasing the pressure on the cathode can reduce the loss of activation polarization potential, thus improving the cell performance” (Yu et al., 2021). Perhaps the most apparent advantage in fuel cell efficiency is its comparison to other propulsion sources: “the efficiency of hydrogen fuel cells is approximately 44%, which is twice higher than that of internal combustion engines” (Pan et al., 2019). Fuel cells in UAVs are efficient, energy dense, and continuously improving with growing literature and flight tests.

2.8 Conclusion

Each part of the system, from flight to fuel, is crucial to the effectiveness of a fuel cell and battery-powered UAV. The fuel cell design of flow channels and material choices impacts the temperature of the system, reaction rates, and cost to build. The battery selection supplies power in high-demand circumstances with rapid response time and contributes to the weight. Storing or producing hydrogen in-flight must address challenges in every state of matter and can be a major limiting factor to flight endurance. Based on the exploratory research of this literature review, it is recommended to adjust the fuel cell flow channels where available to allow for natural temperature regulation and use a platinum catalyst to maximize electrochemical reactions and fuel. The energy management system should incorporate a semi-active configuration of DC-DC converters, and the recent advances in artificial intelligence can also be applicable in training the system to switch between propulsion in different scenarios by incorporating a neural network. A lithium-ion battery supports the system, providing ample power density and energy density for flight. At present, hydrogen pressure vessels holding gas is the most openly accessible storage option, but this choice may impact the mass of the system and inhibit length of missions. Temperature management through coolant and water purging is also recommended. Further adjustments would be necessary for implementation in extreme temperatures or dry climates.

The continuous research and improvement in fuel cell technology opens opportunities to more affordable materials, more sustainable storage, and more flexible missions with heightened endurance and power while reducing overall system weight. Within the fuel cell, experimenting with channel geometry improvements and new catalyst materials may reduce overall cost, and comparing the reaction rate in different fuel cells indicates if the adjustments can still produce electrical energy at a comparable rate to the control. The use of neural networks could adapt to the change of maximum power levels of the battery over time and better manage the battery health life cycles. Exploring hydrogen production for alternate storage avenues could also greatly impact flight endurance. These research openings reflect the growth opportunities in fuel cell applications and the future improvements to address current obstacles in hydrogen fuel cell UAVs.

Chapter 3: Methodology

This section details how the model selection and modification from the original format. It encompasses the digital representation of a physical system by addressing each component in the system. The methodology also discusses the fidelity of the model, including components that are simplified or in a low fidelity representation to achieve a base model while focusing on parameters and changes in the power and mission profile. It outlines the model that is tested and studied for the remainder of this thesis.

3.1 Software Explanation

The simulations and code are within a few MathWorks platforms: MATLAB, Simulink, and Simscape. The first and most basic is MATLAB, a text-based programming language with similar conventions to Python or Java. It relies on scripting, unique syntax rules, and math equations to execute commands. While the overall model screenshot does not show lines of code to the user, the code scripts are running inside each component of the model. MATLAB uses the parameters input by the user and performs data analysis of the simulations.

Simulink, another platform used, is a graphical environment using blocks. These blocks include libraries of logic gates, clocks to measure run time, and sources and sinks. Among these, sources and sinks are two fundamental components of controls experiments. Sources, such as Ramp or Step, can drive the mission profile, and sinks, such as measurement blocks or scopes, capture data from the system response to be analyzed after the simulation. Simulink handles one-way signals, but Simscape can handle components in fluid, thermal, electrical, and more situations. Simscape, the third platform used, is a physical modeling library that exists within Simulink. The

user can connect components such as batteries and motors with wires or connect pumps and compressors through pipes.

The model connectivity across components is achieved through object-oriented programming, where each component is a discrete instance of a physical class. This ability means parts of the program can be multiplied without having to code the sequence again but rather by adding another instance of the class.

The scalability of this format and the variety of blocks included within these programs is best suited for modeling and simulation of the thesis. Additionally, MathWorks provides models of fuel cells, batteries, UAVs, and more alongside documentation to allow the user to change parameters at the surface level all the way to source code. This method is highly customizable based on the testing required and can be simplified or expanded upon depending on desired fidelity and data analysis.

3.2 Original MathWorks Model

The PEM Fuel Cell System model serves as the basis for the fuel cell component of the UAV propulsion system (MathWorks, 2025). This model was created by MathWorks and is very detailed in documentation of each component (Figure 8). The cathode and anode both have very nuanced systems, and the fuel cell is a PEM fuel cell and features the same electrochemical reactions (Equation 1) described in the literature review.

Equation 1

$$2H_2 + O_2 \rightarrow 2H_2O + electricity + heat$$

The anode side supplies the hydrogen reactant from a tank of hydrogen gas with trace amounts of nitrogen. The cathode side supplies the oxygen reactant by capturing atmospheric air and adjusting the pressure and humidity for the reaction. The membrane electrode assembly is also modeled. Excess water can be discarded through a purge valve to prevent moisture damage. Heat generated during operation can be modeled and the model includes a liquid cooling system to prevent overheating. A coolant tank, pump, and radiator make up the liquid cooling system.

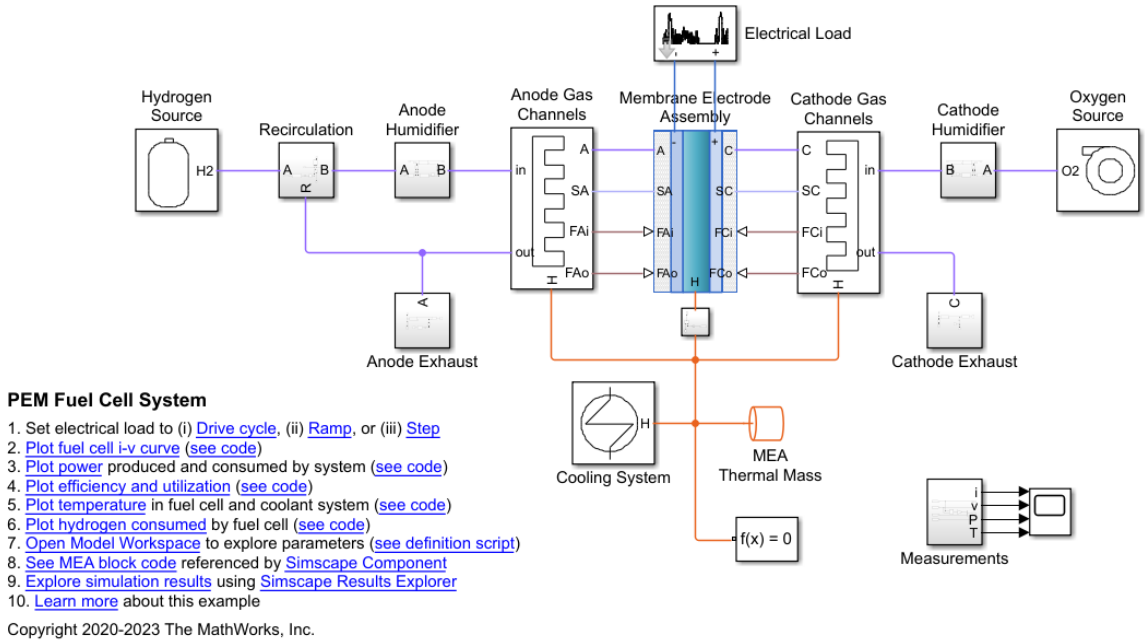

Figure 8 The overall Simulink and Simscape model of a PEM Fuel Cell System (Mathworks, 2025)

3.3 Membrane Electrode Assembly

The MATLAB model documentation describes the MEA programming block as a stack of MEAs within a PEMFC where “hydrogen and oxygen are consumed from the connected anode and cathode flow channels, respectively” (Mathworks, 2025). Further, it specifies that

within a PEMFC, “water vapor is produced at the cathode flow channel. The block also models water transport between the anode and cathode. Waste heat is dissipated to the connected thermal mass” (Mathworks, 2025).

Protons can flow across the MEA, but electrons cannot cross it and instead flow through the external circuit connected to the MEA labeled “Electrical Load” to generate power. Some parameters can be set by the user, such as the number of MEAs in the stack or the thickness of each layer (Figure 9). Others are internal parameters predetermined by MATLAB, such as the gas constants, standard temperature, and standard pressure (Figure 10).

```
parameters
    N_cell       = {400,    '1'     }; % Number of cells in stack
    area_cell    = {280,    'cm^2'  }; % Cell area
    t_membrane   = {125,    'um'    }; % Membrane thickness
    t_gdl_A      = {250,    'um'    }; % Anode gas diffusion layer (GDL) thickness
    t_gdl_C      = {250,    'um'    }; % Cathode gas diffusion layer (GDL) thickness
    io           = {8e-05, 'A/cm^2'}; % Exchange current density
    iL           = {1.4,    'A/cm^2'}; % Max (limiting) current density
    alpha        = {0.5,    '1'     }; % Charge transfer coefficient
    D_H2O_gdl_A  = {0.07,   'cm^2/s'}; % Water vapor diffusivity in anode GDL
    D_H2O_gdl_C  = {0.07,   'cm^2/s'}; % Water vapor diffusivity in cathode GDL
    rho_membrane = {2000,   'kg/m^3'}; % Density of dry membrane
    M_membrane   = {1.1,    'kg/mol'}; % Equivalent weight of dry membrane
end
```

Figure 9 The user-defined default parameters in the MATLAB source code within the MEA Simscape block (Mathworks, 2025)

```
% Internal parameters
parameters (Access = protected)
    % Constants
    R_u    = {8.31446261815324, 'J/K/mol'}; % Universal gas constant
    F      = {96485.33212,      'C/mol'  }; % Faraday constant
    G_H2O  = {-237.14,          'kJ/mol' }; % Gibbs free energy of water
    HHV_H2 = {285.8,            'kJ/mol' }; % Higher heating value of hydrogen
    LHV_H2 = HHV_H2 - MW_H2O * hfg_H2O_std; % Lower heating value of hydrogen
    T_std  = {25,               'degC'   }; % Standard temperature
    p_std  = {1,                'atm'    }; % Standard pressure

    % Standard cell potential
    E_cell = G_H2O/(-2*F);

    % Membrane permeability to water
    K_darcy = {1.58e-14, 'cm^2'};

    % Compute molar masses from specific gas constants
    MW_H2O = R_u/C.R_w;
    MW_O2  = R_u/C.R_g;
    MW_H2  = R_u/A.R_g;
```

Figure 10 The internal parameters in the MATLAB source code within the MEA Simscape block (Mathworks, 2025)

Before beginning the list of equations within the code using the parameters, it can be helpful to recognize the physical meaning and importance of the constants and variables. F denotes Faraday's constant measured in coulombs per mole of electrons (96485 C/mol) and G is Gibb's free energy of water. Gibb's free energy measures the amount of useful work that can be done by a system and is dependent on entropy and enthalpy. Faraday's constant in the calculations helps to measure the electrical amount of charge from the chemical reaction and work.

There are also higher heating values (HHV) and lower heating values (LHV) for each substance. In the equations listed in the table below, the HHV and LHV of hydrogen are relevant to the fuel cell. "[HHV] is the enthalpy difference between the reactants and the products per unit mass of fuel when the water that is produced leaves as liquid" and "includes the latent heat of condensation of the water vapor" (Mitchell & Braun, 2013). However, LHV "is the enthalpy

difference between reactants and products per unit mass of fuel when the water formed by the combustion process leaves as a vapor," which is why the LHV equation uses latent heat of vaporization rather than condensation (Mitchell & Braun, 2013).

The Mathworks model MEA block incorporates the following equations (Table 1) to analyze the PEM fuel cell system, and a description of each equation is also provided (Mathworks 2025 & Hartless 2022).

Table 1 Model Equations

#	Formatted Equation	Parameters & Variables	Brief Explanation
1	$E = \frac{-\Delta G_{H2O}}{nF}$	E: Std. Potential (V) ΔG_{H2O}: Gibbs Free Energy of water n: Electrons per mole F: Faraday's Constant	Calculates the standard cell potential using the thermodynamic quality Gibbs free energy of water set at -237.14 kJ/mol and Faraday's constant.
2	$P_{elect} = N_{cell} \cdot V_{cell} \cdot i_{cell} \cdot A_{cell}$	P_{elect}: Electrical Power (W) N_{cell}: Number of cells V_{cell}: Cell Voltage (V) i_{cell}: Current density (A/m²)	Determines total electrical power produced by the stack.

#	Formatted Equation	Parameters & Variables	Brief Explanation
		A_{cell}: Active area (m^2)	
3	$P_{diss} = I_{st}(E_{nernst} - V_{fc})$	P_{diss}: Heat Power (W) E_{nernst}: Reversible Potential (V) V_{fc}: Cell Voltage (V)	Calculates power lost as heat (dissipated) from the system.
4	$\eta_{HHV} = \frac{V_{fc}}{HHV}$	η_{HHV}: Thermal Efficiency V_{fc}: Cell Voltage (V) HHV: Higher Heating Value voltage	Thermal efficiency based on the Higher Heating Value (HHV) of hydrogen.
5	$\eta_{LHV} = \frac{V_{fc}}{LHV}$	LHV: Lower Heating Value voltage	Thermal efficiency based on the Lower Heating Value (LHV) of hydrogen.
6	$HHV = LHV + H_{vap}$	HHV/LHV: Heating Values H_{vap}: Enthalpy of Vaporization	Relationship between Higher and Lower Heating Values of hydrogen.

#	Formatted Equation	Parameters & Variables	Brief Explanation
7	$\dot{m}_{cons} = \frac{I \cdot M}{nF}$	$\dot{m}_{cons}$: Mass flow (kg/s) M: Molar mass (kg/mol) I: Current (A)	Calculates the mass consumption rate of hydrogen or oxygen.
8	$\dot{m}_{w,gen} = \frac{I \cdot M_w}{2F}$	$\dot{m}_{w,gen}$: Water production rate M_w: Molar mass of water	Determines the mass rate of water produced by the reaction.
9	$N_w = N_{diff} + N_{drag} + N_{pres}$	N: Molar flux (mol/s·m²) $diff/drag/pres$: Transport modes	Total water transport across the membrane due to diffusion, drag, and pressure.
10	$RH = \frac{P_{wv}}{P_{sat}}$	RH: Relative humidity P_{wv}: Water vapor pressure P_{sat}: Saturation pressure	Ratio of actual pressure to water vapor saturation pressure.
11	$a_i = x_i \cdot \frac{P}{P_{std}}$	a_i: Activity x_i: Mole fraction	Calculates the activity of hydrogen or oxygen based on mole fraction and pressure.

#	Formatted Equation	Parameters & Variables	Brief Explanation
		P/P_{std}: Operating/Std pressure	
12	$a_{w,ca} = \frac{x_{w,ca}P_{ca}}{P_{sat}}$	ca: Cathode subscript $x_{w,ca}$: Water mole fraction	Calculates water activity at the cathode.
13	$E_{nernst} = E^0 + \frac{RT}{nF}\ln\left(\frac{a_{H2}\sqrt{a_{O2}}}{a_{H2O}}\right)$	R: Gas constant T: Temperature (K)	The Nernst voltage, representing reversible open-circuit potential.
14	$B = \frac{RT}{\alpha nF}$	B: Tafel slope α: Transfer coefficient	Activation loss coefficient derived from the Tafel equation.
15	$V_{act} = B\ln\left(\frac{i}{i_0}\right)$	i: Current density (A/m²) i_0: Exchange current density	Voltage loss due to activation polarization.
16	$V_{conc} = \frac{RT}{nF}\ln\left(1 - \frac{i}{i_L}\right)$	i_L: Limiting current density	Concentration losses when current is below the limiting density.
17	$V_{conc} = \beta\exp(ci)$	β, c: Empirical coefficients	Concentration losses when current exceeds limiting density.

#	Formatted Equation	Parameters & Variables	Brief Explanation
18	$\lambda = a + b(RH)$	λ: Membrane water content a, b: Linear constants ($RH < 0$)	Humidity parameter when relative humidity is less than 0.
19	$\lambda = a + b(RH) + c(RH)^2 + d(RH)^3$	a, b, c, d: Polynomial constants	Humidity parameter for RH between 0 and 1.
20	$\lambda = a + b(RH - 1)$	a, b: Linear constants ($RH > 1$)	Humidity parameter when relative humidity is greater than 1.
21	$R_m = \frac{t_m}{\sigma_m}$	R_m: Resistance ($\Omega \cdot m^2$) t_m: Membrane thickness	Total ohmic resistance of the membrane.
22	$\sigma_{ref} = a\lambda - b$	σ_{ref}: Conductivity at T_{ref} a, b: Empirical parameters	Membrane conductivity parameter at a reference temperature.
23	$\sigma_m = \sigma_{ref} e^{c\left(\frac{1}{T_{ref}} - \frac{1}{T}\right)}$	c: Activation energy constant	Temperature-dependent membrane conductivity.
24	$V_{ohm} = i \cdot R_m$	i: Current density (A/m^2)	Voltage loss due to ohmic resistance.

#	Formatted Equation	Parameters & Variables	Brief Explanation
25	$D_w = D_{ref} e^{c\left(\frac{1}{T_{ref}} - \frac{1}{T}\right)}$	D_w: Diffusion coefficient c: Constant	Water diffusion coefficient across the membrane.
26	$C_w = \frac{\rho_{m,dry}}{M_m}$	$\rho_{m,dry}$: Density M_m: Equivalent weight	Water concentration at the catalyst layers.
27	$N_{diff} = D_w \frac{dC_w}{dz}$	z: Spatial coordinate	Molar flux of water due to diffusion.
28	$n_d = \frac{a\lambda}{b}$	n_d: Drag coefficient a, b: Constants ($\lambda \ge 0$)	Electro-osmotic drag coefficient for $\lambda \ge 0$.
29	$n_d = c$	c: Alternative constant	Electro-osmotic drag coefficient (alternative).
30	$N_{drag} = n_d \frac{i}{F}$	i: Current density	Molar flux of water due to electro-osmotic drag.
31	$x_{w,i} = \frac{P_{sat} RH_i}{P_i}$	$x_{w,i}$: Mole fraction at layer i	Water vapor mole fraction at the catalyst layers.
32	$N_{w,an} = \frac{P}{RT} \frac{D_{w,an}}{t_{an}} \Delta x_w$	t_{an}: Anode GDL thickness	Molar flux of water across the anode diffusion layers.

#	Formatted Equation	Parameters & Variables	Brief Explanation
33	$N_{w,ca} = \frac{P}{RT}\frac{D_{w,ca}}{t_{ca}}\Delta x_w$	t_{ca}: Cathode GDL thickness	Molar flux of water across the cathode diffusion layers.
34	$N_{pres} = K_p \frac{\Delta P}{t_m}$	K_p: Permeability ΔP: $P_{an} - P_{ca}$	Hydraulic water flux when anode pressure is higher.
35	$N_{pres} = -K_p \frac{\Delta P}{t_m}$	t_m: Membrane thickness	Hydraulic water flux when cathode pressure is higher.
36	$\dot{\mathrm{Q}}_{\mathrm{react}} = \dot{\mathrm{n}}_{\mathrm{H2}}\Delta \mathrm{H}^0$	$\dot{n}_{H2}$: Molar flow ΔH^0: Reaction enthalpy	Energy generation rate due to reaction at standard temperature.
37	$\dot{Q}_{sens} = \sum \dot{m}_i C_{p,i} \Delta T$	$C_{p,i}$: Specific heat ΔT: $T - T_{std}$	Energy gain from bringing reactants/products to standard temperature.
38	$\dot{Q}_{mem} = N_w M_w C_{p,w} \Delta T$	M_w: Molar mass water	Energy gain in the membrane due to water transport.
39	$\dot{Q}_{net} = \dot{Q}_{react} - P_{elect} - \dot{Q}_{loss}$	$\dot{Q}_{loss}$: External heat loss	Total net energy gain in the stack.
40	$L_{ch} = \frac{W_{st}}{2}$	W_{st}: Stack width	Assumed length of gas channels (half the stack width).
41	$A_{ch} = w_{ch} \cdot d_{ch}$	w_{ch}, d_{ch}: Channel dimensions	Cross-sectional area calculation for gas channels.

#	Formatted Equation	Parameters & Variables	Brief Explanation
42	$\dot{m}_{air,cmd} = \frac{SR \cdot I \cdot N \cdot M_{air}}{4F \cdot y_{O2}}$	SR: Stoic. ratio; N: Cells y_{O2}: Oxygen fraction	Target mass flow rate for the air compressor.
43	$G(s) = \frac{Ke^{-\tau s}}{Ts + 1}$	τ: Delay; T: Time constant	Transfer function used for signal delay in control systems.
44	$\dot{m}_{corr} = \dot{m}_{act} \frac{\sqrt{T/T_{std}}}{P/P_{std}}$	act: Actual; std: Standard	Corrected mass flow rate calculation for the compressor.
45	$A_v = \frac{\dot{m}}{C_d\sqrt{2\rho\Delta P}}$	C_d: Discharge coefficient ρ: Density	Calculation for the restriction area of the pressure reducing valve.
46	$\dot{m}_{rec} = \epsilon \cdot \dot{m}_{cons}$	ϵ: Recirculation ratio	Calculation for recirculated hydrogen mass flow rate.

3.4 Gas Channels

Within the model, there is a block representing the anode gas channels and a block representing the cathode gas channels. When selected, the model will open the block and show a subsystem as seen below in Figure 11.

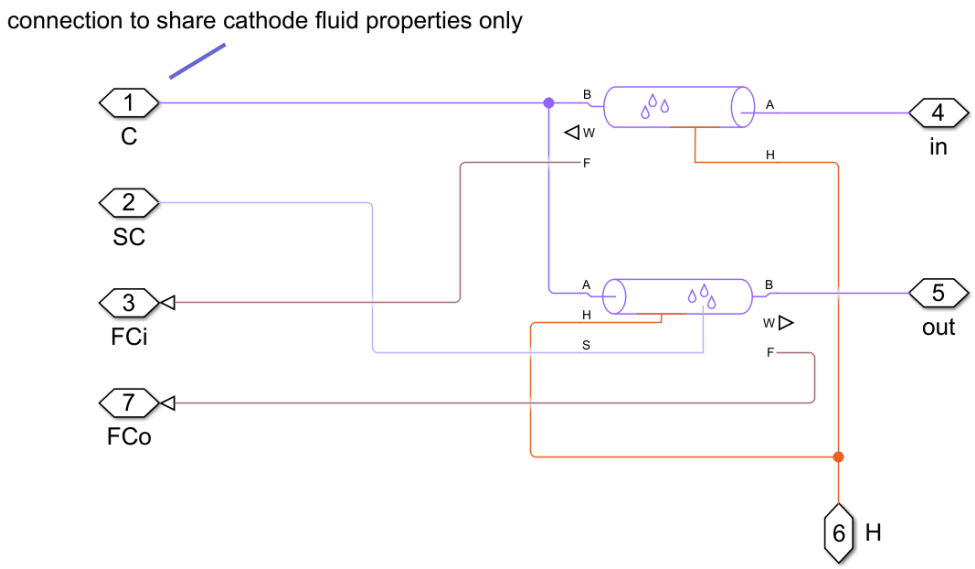

Figure 11 The cathode gas channels subsystem (MathWorks, 2025)

The connection ports on each side of the subsystem link other blocks, such as the MEA and more. There are two moist air pipes within each gas channels block. The moist air pipe Simscape block models flow through a pipe while considering losses from friction and heat transfer through the pipe wall within a moist air network (MathWorks 2025). “The pipe contains a constant volume of moist air. Pressure and temperature vary dynamically based on the net mass and energy accumulation” (MathWorks, 2025). It is also important to note the gas source that is connected to the gas channel. On the left side of the model, the hydrogen source supplies the anode gas channels, while on the right side of the model, the oxygen source supplies the cathode gas channels.

The cathode exhaust block expels waste such as liquid water (the main product of the electrochemical reaction), water vapor, heat, and oxygen depleted air, which is mostly nitrogen. This exhaust supports a conducive humidity and temperature for the fuel cell to safely operate. On the anode side, the anode exhaust block is accompanied by a recirculation block. The recirculation block recycles unconsumed hydrogen in the electrochemical reaction so it can be

used as fuel. If there is a large amount of excess hydrogen, it can be purged through the exhaust block. Back-diffusion and nitrogen crossover are also concerns, where substances from the cathode side migrate to the anode side. This means the anode exhaust block also handles removal of water and nitrogen as needed.

Each side has a humidifier block, as seen by the cathode humidifier and anode humidifier. Another component within the humidifier subsystem is the measurement selector block, which "extracts the moist air volume measurements reported by the physical signal port F of moist air blocks" and elaborates that "physical signal ports P [Pa], T [K], W, G, and D report the pressure, temperature, moisture level, trace gas level, and mass ratio of water droplets to moist air, respectively, of the connected moist air volume" (Mathworks 2025). Each port communicates a value that represents a variable and can be measured through MATLAB plots and connected to other blocks for analysis in thermal, electrochemical, or fluid contexts. Both humidifiers also contain a moisture source block, which can be a source or sink depending on if moisture is added or removed. The block allows the user to set mass flow rate of moisture in kilograms per second and temperature of moisture in Kelvin, and the moisture can be water vapor or liquid water (Mathworks 2025).

3.5 Oxygen Source

The oxygen source block, represented by a fan icon on the right side of the model, houses the subsystem shown in Figure 12 below. The air properties block and air intake block assume moist air as the given substance, which is composed of dry air, water vapor, and trace gas. Moist air is 78% nitrogen, 21% oxygen, and 1% trace gases (Schlesinger & Bernhardt, 2020). The compressor facilitates the movement of oxygen through the tubes and towards the gas channels and MEA. The final step before the O2 block that connects to other systems is the flow rate

sensor block, which records “the mass flow rate, volumetric flow rate, energy flow rate, water vapor mass flow rate, trace gas mass flow rate, and water droplets mass flow rate” of the oxygen through Simscape physical signal ports (Mathworks 2025). This sensor ensures the conservation of mass and energy as the oxygen travels through the cathode side of the model.

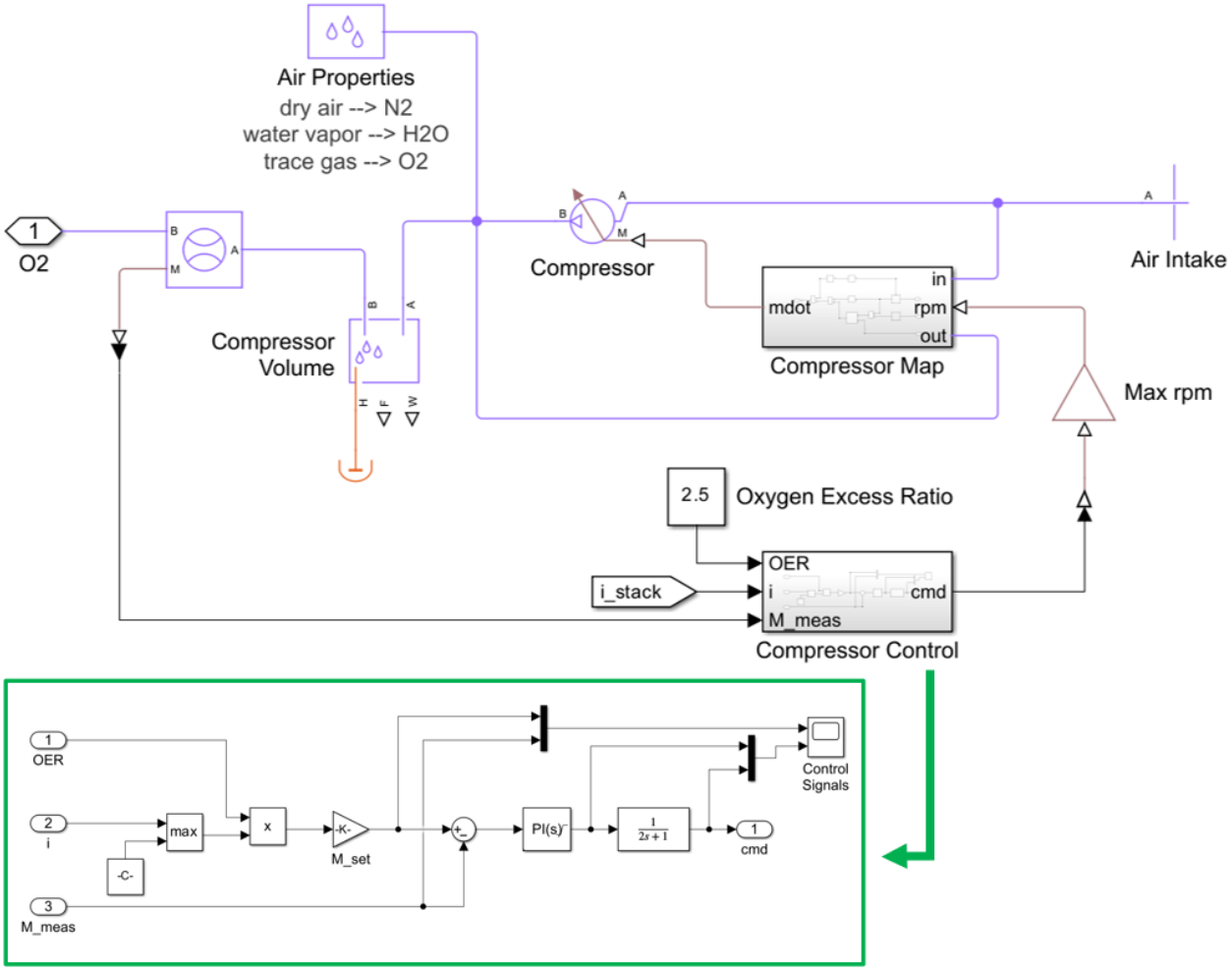

Figure 12 The oxygen source subsystem (Mathworks, 2025)

3.6 Hydrogen Source

Hydrogen is stored in a high-pressure tank, but it needs to be at a much lower pressure for fuel cell operations. The model subsystem shows this process in Figure 13 below. On the fuel tank block, under the initial condition settings, the default pressure is 70 MPa and default

temperature is 20 degrees Celsius. The stack pressure and environmental pressure are added together to serve as the set pressure in the pressure-reducing valve block. After that process, the pressure of hydrogen has decreased significantly, as the pressure within the pipe is only 0.10132 MPa and the stack pressure is 0.16 MPa. The fuel properties block simulates a moist air network for system operations, and the moist air network in this case is the atmosphere.

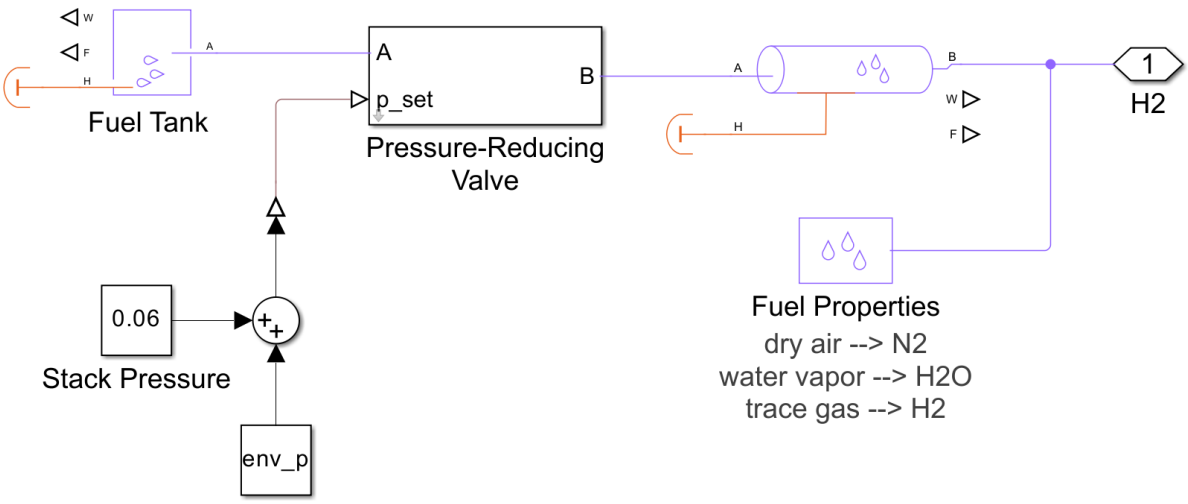

Figure 13 The hydrogen source subsystem (Mathworks, 2025)

3.7 Cooling System

The cooling system block houses a subsystem to control the heat of the system (Figure 14). Between the MEA block and the cooling system block is a heat dissipation block. It houses a heat flow rate sensor, which records the flow rate across the sensor and assigns this value to the variable Q_stack. The MEA thermal mass block "models internal energy storage in a thermal network. The rate of temperature increase is proportional to the heat flow rate into the material and inversely proportional to the mass and specific heat of the material" (Mathworks 2025). Across from the MEA thermal mass block is the cooling system. The results of the subsystem are viewed in the pump control. Within the pump control block, the user can track a graph of the fuel

cell stack temperature and see the calculations of differences in theoretical and experimental temperature used to generate the graphs. The cooling system includes a tank of coolant, a block to specify the properties of the coolant, fuel cell coolant channels, a radiator, and temperature sensors throughout the subsystem.

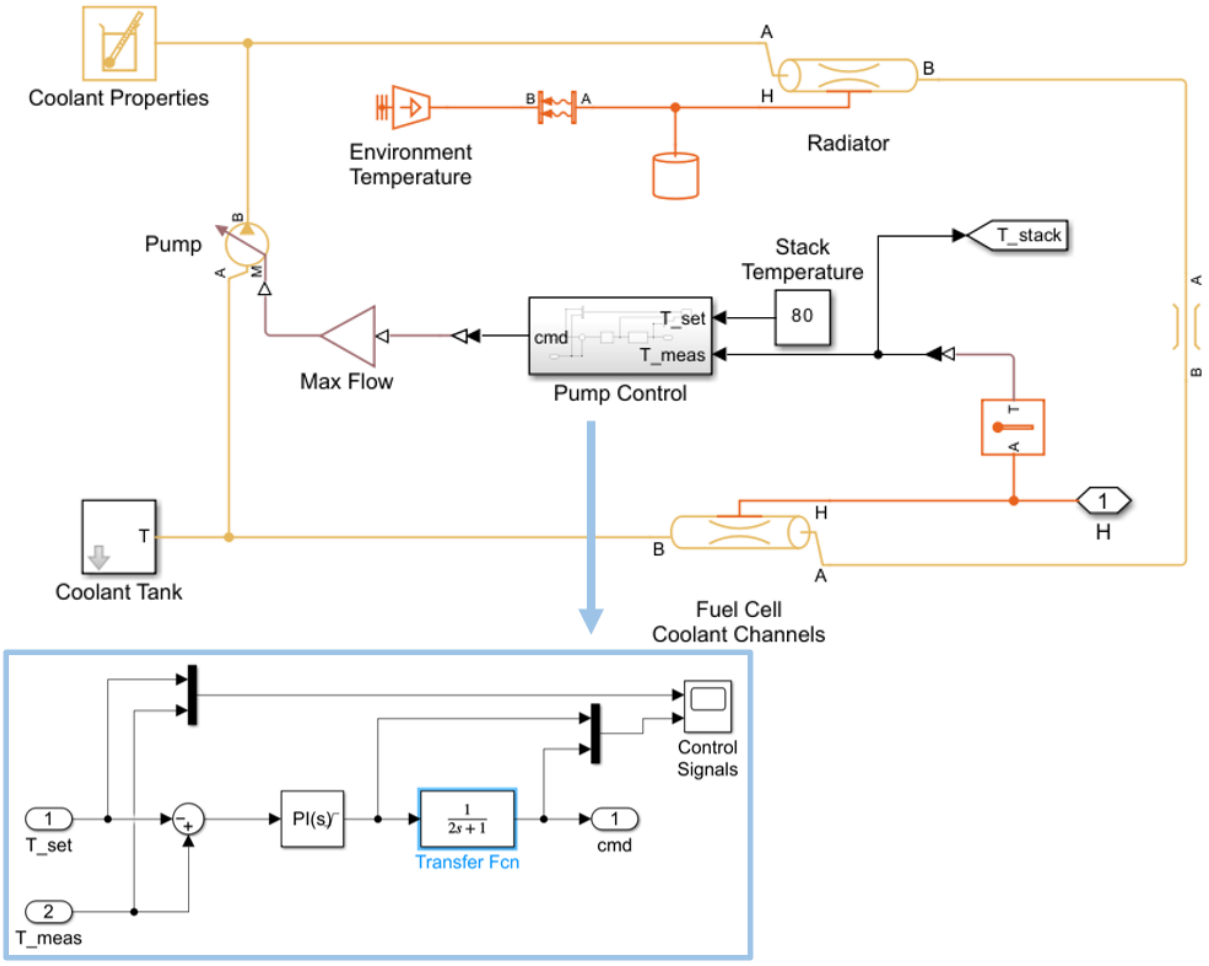

Figure 14 The cooling subsystem (Mathworks, 2025)

3.8 Battery Model

While the fuel cell model is a high-fidelity model with thermal, moisture, and electrical management, the battery model is a low-fidelity model. This means that cooling systems, waste management, and other detailed subsystems are not fleshed out in the battery model. Instead, this

study focuses on the power generation in a simple circuit incorporating a battery or battery pack. These components operate in a circuit that requires a resistor and an electrical reference, often called ground. Outside of physical components, sensors including the voltage sensor (V) and current sensor (I) transmit these values to a measurement scope block, which generates graphs of each of these variables over time. Another important tool is the physical signal to Simulink converter, shown by the two black and white triangles. This tool changes a Simscape physical quantity, such as current in amps, to mathematical signals that can be understood by Simulink and the scope block. The voltage, current, and product of these variables, power, are all essential metrics to track in the model.

At first, the model used a basic circuit with a single Simulink block called the Battery Equivalent Circuit block (Figure 15). Surrounding the battery block are other sensors and circuit components. The block with the “V” connected in parallel with the battery is a voltage sensor block to measure the potential difference across the circuit. The block with an “A” connected in series with the battery is a current sensor block to measure the flow of electricity within the circuit. To the right of the current sensor is a resistor, which consumes energy from the battery. The final block in the circuit is the solver configuration, represented by $f(x) = 0$, and it specifies numerical solver settings in the Simscape model. The small triangle under the battery is also required; it is a zero-voltage reference point and the solver configuration needs this reference in order to calculate the data for the simulation. The arrows convert physical signals to Simulink signals, which is necessary as Simulink signals are the required inputs for the measurement scope, the block furthest to the right. This scope acts as an oscilloscope, and the voltage and currents are both inputs, alongside their product, power.

The Battery Equivalent Circuit block is different than the Battery (Table-Based) block because it has less parameters to set and is a lower fidelity model. These two blocks represent battery cells and faced challenges generating the power for a UAV mission. Through assessing power demands of a UAV and taking suggestions from MathWorks customer support engineers, it was decided that a battery pack should be used in the simple circuit rather than a battery cell block (Figure 16). Rather than the battery block symbol, the battery pack named “Thesis 1 Pack” replaces this component as a power source. The other circuit elements, signal converters, and measurement devices remain the same.

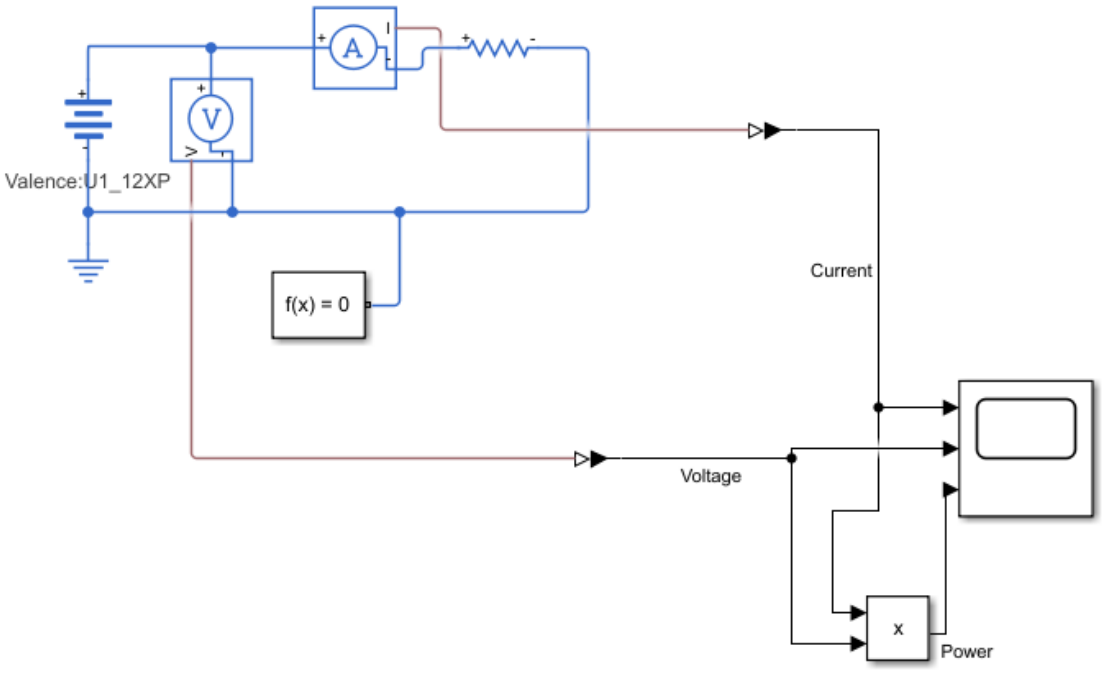

Figure 15 Battery Cell Model

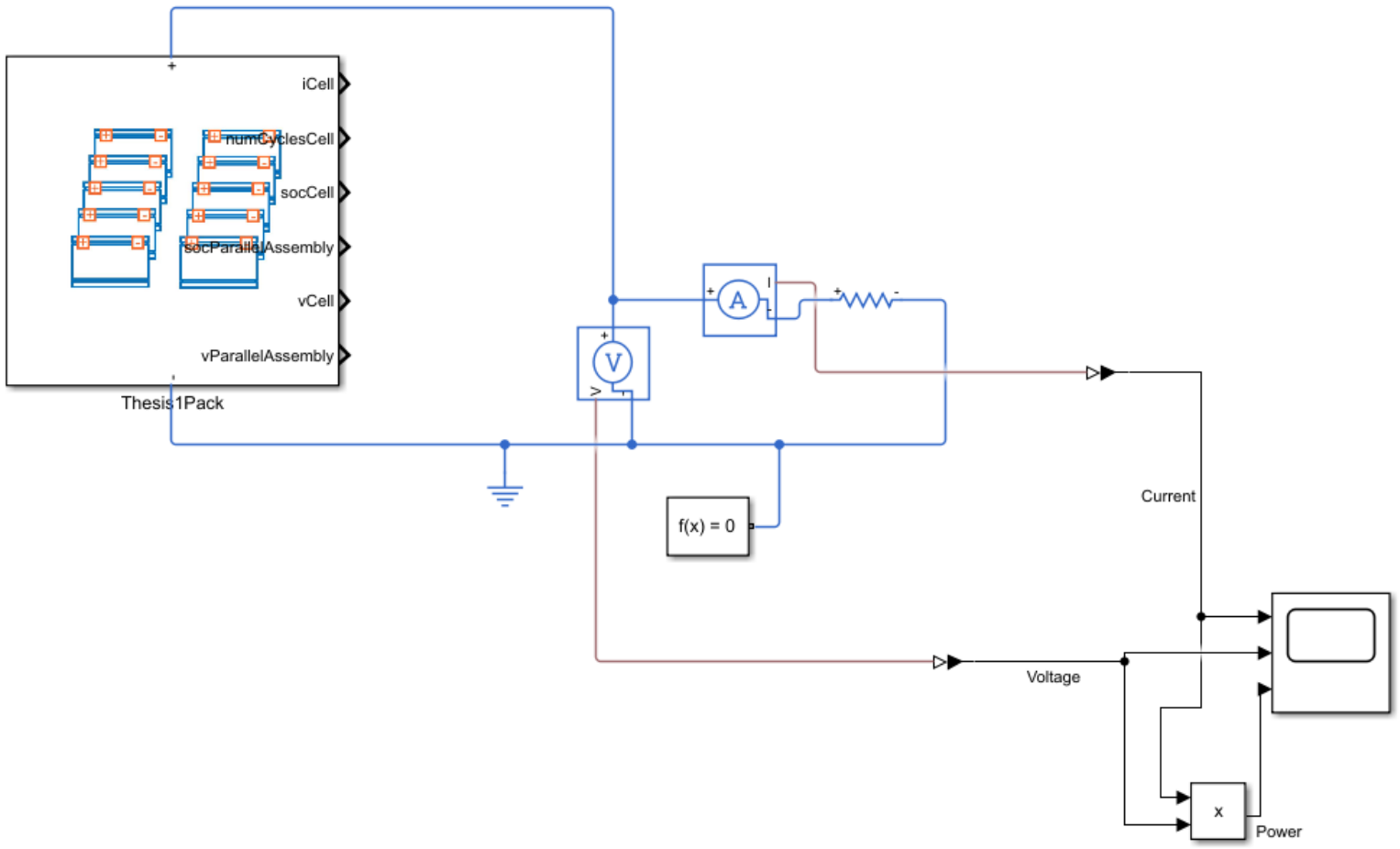

Figure 16 Battery Pack Model

The Simulink Battery Builder app allows users to create a battery pack by starting with a cell and building further into parallel assemblies, modules, module assemblies, and finally, a pack (Figure 17). A battery pack includes cells in series and parallel circuit paths, creating a complex circuit, to generate more power. While a cell could not generate enough power to complete a UAV mission, a pack is more suited to this power demand. The Battery Builder app also includes selections for electrical properties, geometry, and thermal modeling. The battery pack in this model uses a lumped setting, which is a lower fidelity approach than considering individual cells and their thermal output. This creates faster simulations and simplifies model evaluation. The options on the side of the block can measure state of charge, number of cycles, and additional metrics at the cell or parallel assembly level. In this research, the measurements are taken at the pack level, and the battery pack is connected the positive and negative ports while the side ports remain unused. A measurement scope in the larger model reads the voltage, current, and power of the battery.

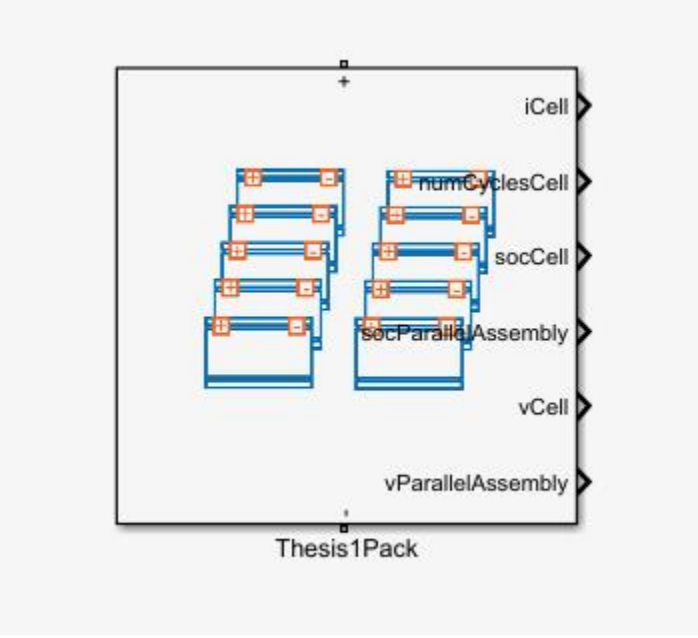

Figure 17 A Battery Pack Block in Simulink after exporting from the Simulink Battery Builder app

These battery models are tested individually to ensure efficiency prior to integration into the larger system model (Figure 18 & Figure 19). The previously described models are integrated into the right side of the model, while the original fuel cell components remain on the left. The model with battery blocks includes two block components so that the power can be doubled. The battery pack includes several battery cells. The other circuit components remain the same. The solver configuration block on the battery side is disconnected because the fuel cell is connected to a solver configuration block already, and the model must only have one solver configuration block. Some key indicators of a sound model include measurements such as voltage and current displayed on the measurement scope and lack of errors within MATLAB while running the model.

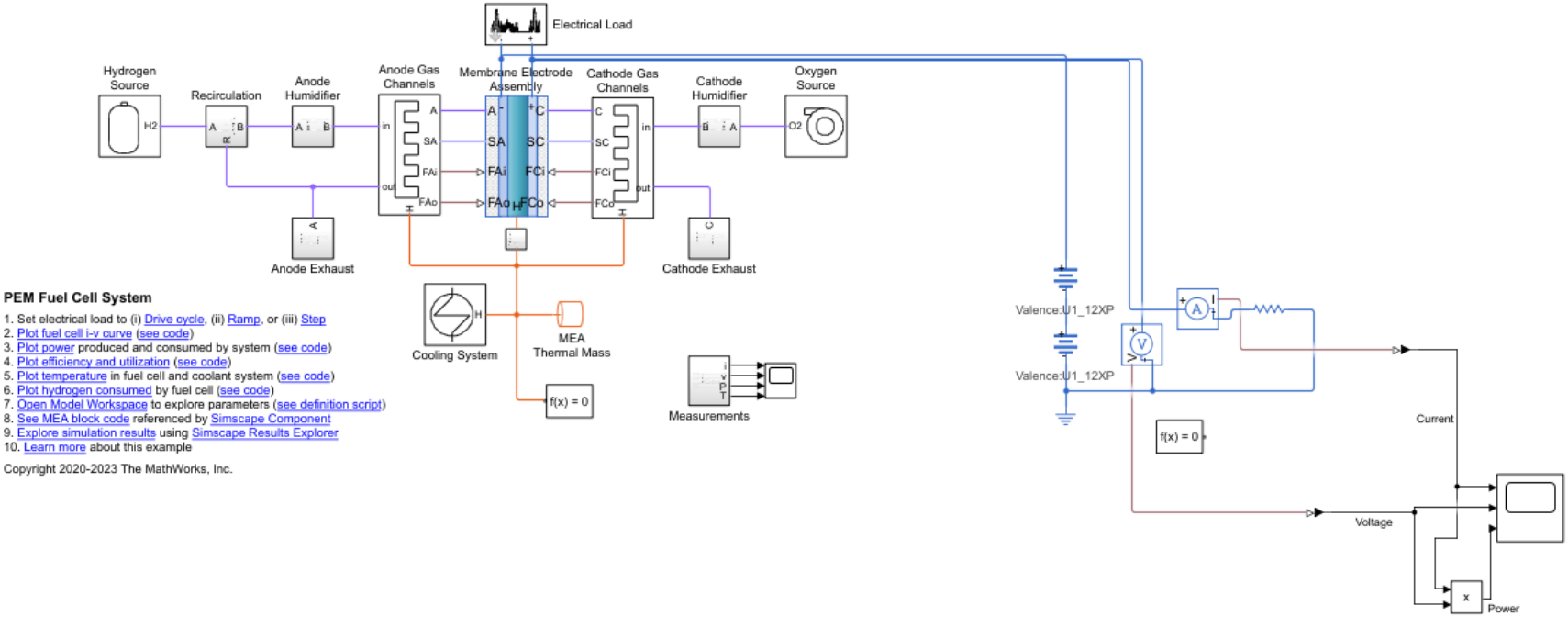

Figure 18 Full model with 2 battery cells

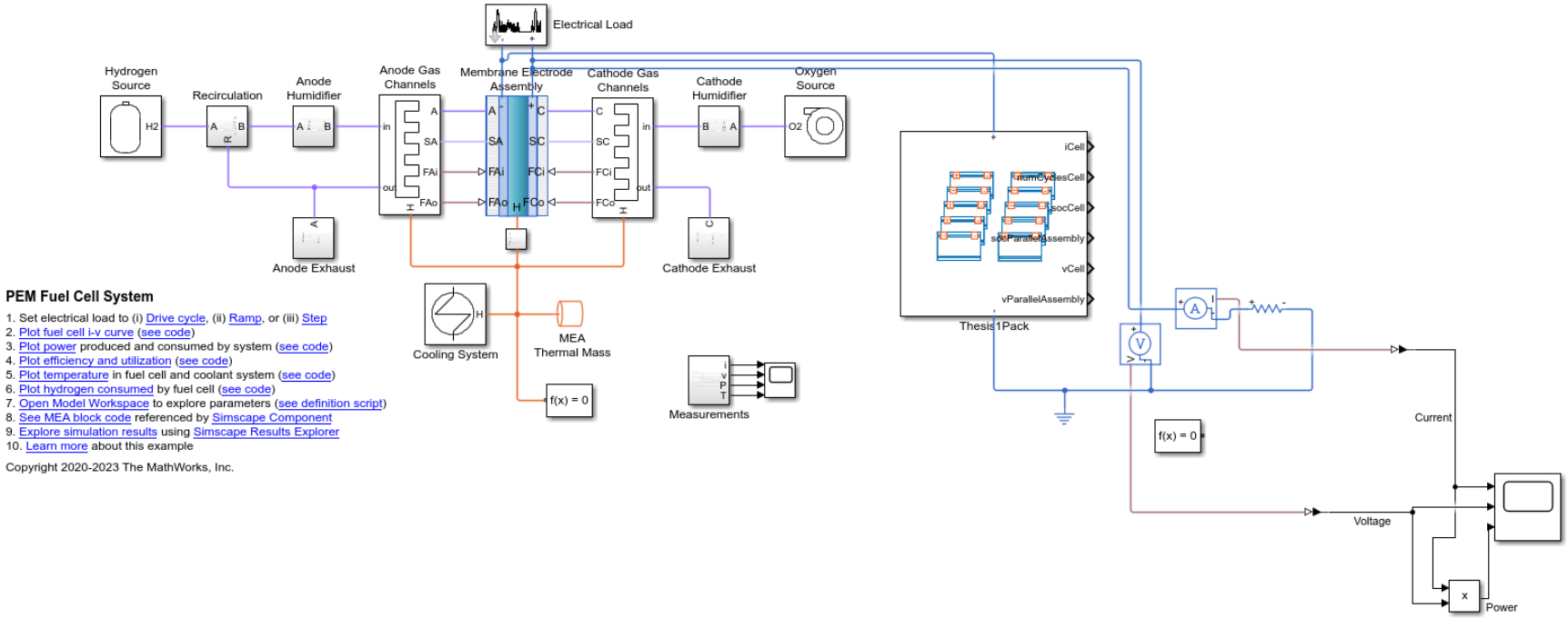

Figure 19 Full model with battery pack integrated

The combination of a detailed fuel cell model developed by MathWorks and a simple battery circuit incorporating a battery pack developed for this project combine to form the overall model of this thesis. The next chapter will demonstrate the models and results of those described above.

Chapter 4: Testing

This section details the model as it is run in individual sections and as a complete model, along with the simulation results. The fuel cell and battery models are each run separately, and the results are then compared. The integrated model runs with both power sources, showing a hybrid system, and this result is compared to the previous ones.

4.1 Drive Cycle and Power

The UAV flies for two hours with a cruise altitude of 350 ft. This time limit is chosen because applications in surveying agriculture and military surveillance generally fall near or within this timeframe. The altitude remains under the maximum allowable limit of 400 ft in the U.S. for UAV flight. The mission includes takeoff, climb, cruise, descent, and landing. The UAV includes a camera for surveillance, and the UAV weight is assumed to be 7 kg including the camera for testing purposes. This weight is similar to the weight of UAVs studied in the literature review. The connection between the mission profile and the model is the Electrical Load block. This model has options for the electrical load to be a ramp, step, or drive cycle format. The drive cycle method is the way to simulate power demand that changes over time, with spikes of power and various changes of power needs throughout the mission. The drive cycle file contains a drive cycle power data set and a drive cycle time data set. When the power data set and drive cycle time data set are plotted together, this shows the power needed over a given amount of time in seconds. Both data sets are stored as matrices and incorporated in the inputs section of the Electrical Load block. The first set of model simulations use the drive cycle from the original MathWorks model. Future simulations can incorporate custom mission profiles tailored to the UAV.

The scopes within the model capture voltage, current, power, and fuel cell stack temperature. A separate code section graphs the thermal efficiency of the fuel cell based on HHV and LHV as well as efficiency based on percentage of reactants used. A scope on the battery side captures power, voltage, and current.

4.2 Fuel Cell Only Testing

Problems in the initial testing stages included the failure of the simulation due to algebraic errors, not meeting initial conditions, and failure to converge. Initial conditions are guidelines to ensure the equipment is safe. They control temperature and humidity ranges, among other operating parameters. When an overwhelming power demand reaches the system, the strain can cause unsafe high temperatures and cause the simulation to run outside initial conditions and fail. Here, the initial conditions within the hydrogen storage system of the fuel cell likely could not be met due to demand on the system for more fuel. In addition, it is possible that a variable was mislabeled or following an incorrect tag between the MATLAB code and Simulink model, causing a failure to converge.

The model workspace within Simulink and the base workspace in MATLAB each contain constants, variables, matrices, and other factors. It is vital to understand where the model is pulling each value from and how that could impact the simulation. The below graph shows an example from a failed simulation where the model did not run for the full 7200 seconds due to an algebraic error in the simulation solver and issues with the drive cycle power demand (Figure 20). The efficiency and reactant use graphs also stopped early due to the simulation failure (Figure 21). The physical implications of a failure could include the UAV engine failing mid-flight due to unsafe temperatures or consuming all the available hydrogen for fuel. When a simulation error flags a temperature, moisture level, or hydrogen level below the minimum or

above the maximum, it is more than a mathematical concern. These safe operating ranges are implemented to ensure that the simulation can run for the full amount of time, and that a UAV could safely complete a flight mission in real-world applications.

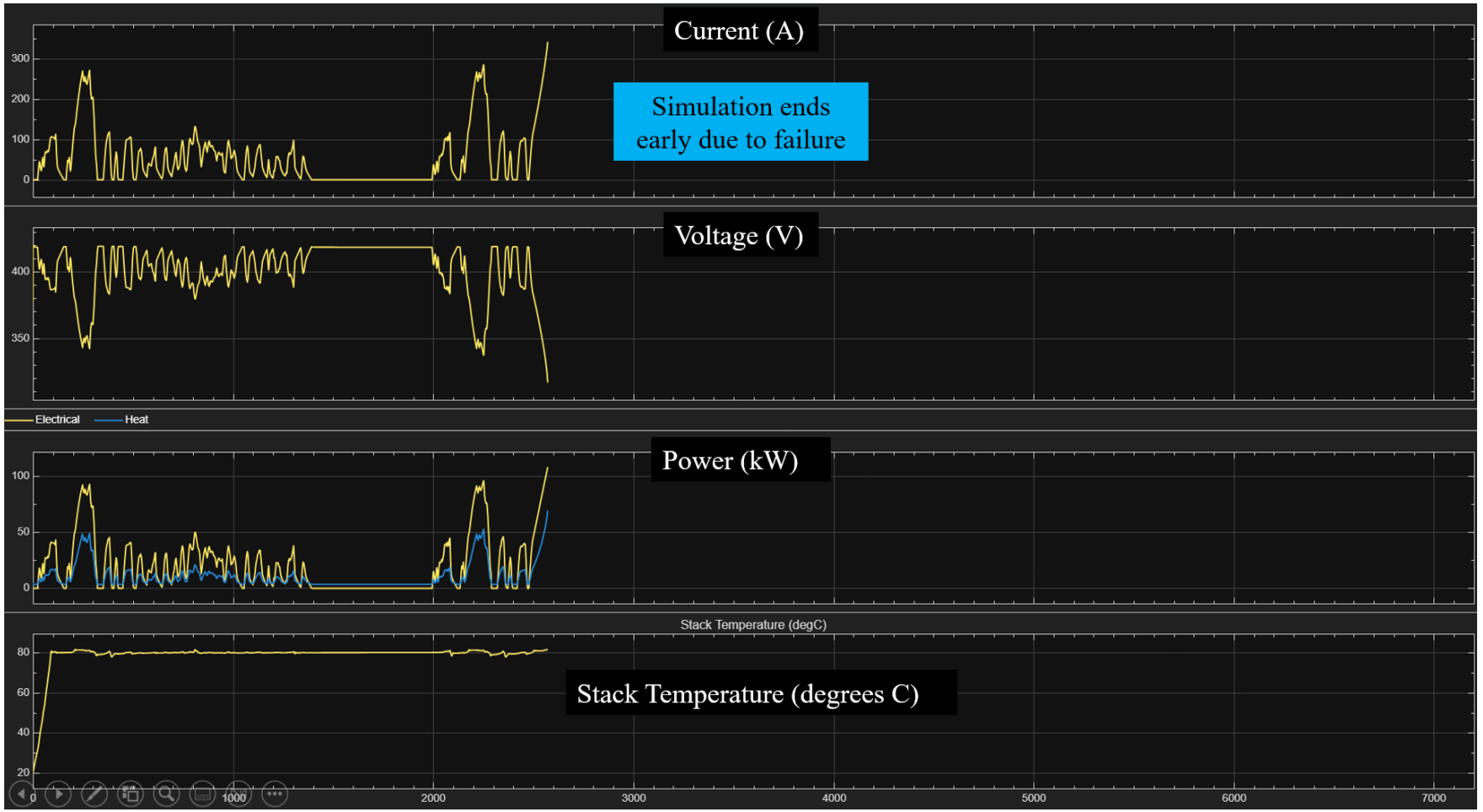

Figure 20 Example data from a simulation that fails at 2573.166 s

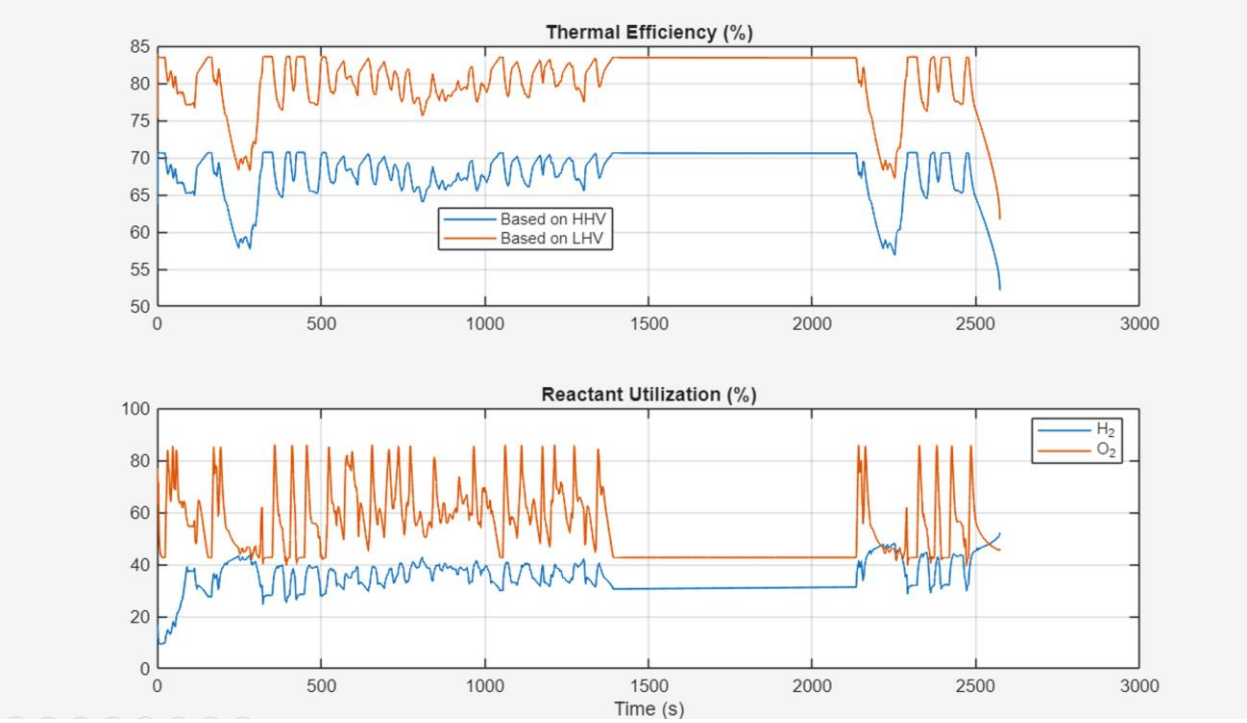

Figure 21 Fuel cell efficiency data prior to failure at 2573.166 s

In troubleshooting the failure, isolating the system with the error is important. Each block is supported by code in the MATLAB file. Similar to commenting out lines of code so that they do not run with the rest of the program, model blocks can be commented out as well. The battery, sensors, and scope on the battery side were all commented out on the model. This allowed specific troubleshooting on the fuel cell side with the drive cycle and electrical load. The failure persisted until the default drive cycle file was replaced with a new drive cycle. The new cycle repeated the original matrix values for multiple cycles to lengthen the amount of data and time. This gave enough data to fill the drive cycle for a full 7,200 seconds, or 2 hours, of simulation. The graph below shows the measurement scope on the fuel cell side and the efficiency when tested with 400 fuel cells in the stack (Figure 22 & Figure 23). The battery is

commented out for this initial round of testing to ensure the failure related to the drive cycle is resolved.

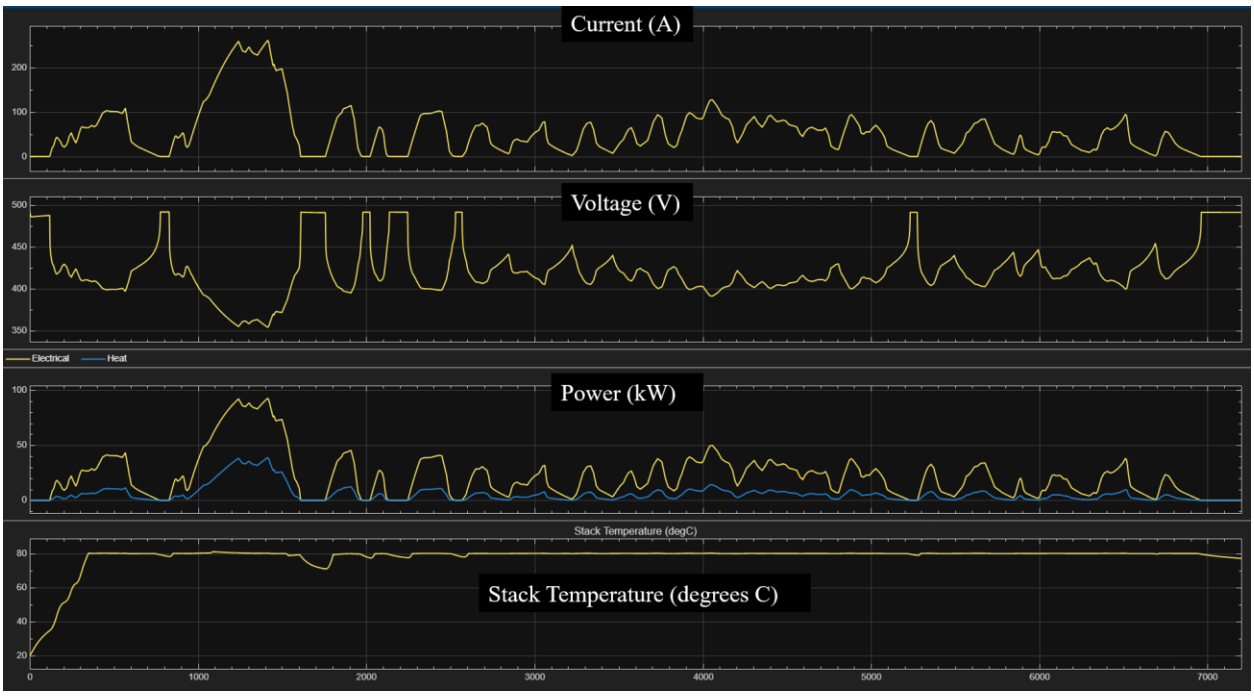

Figure 22 Data from a fuel-cell-only run (battery commented out) using 400 cells in the stack for 7200 s, or 2 h

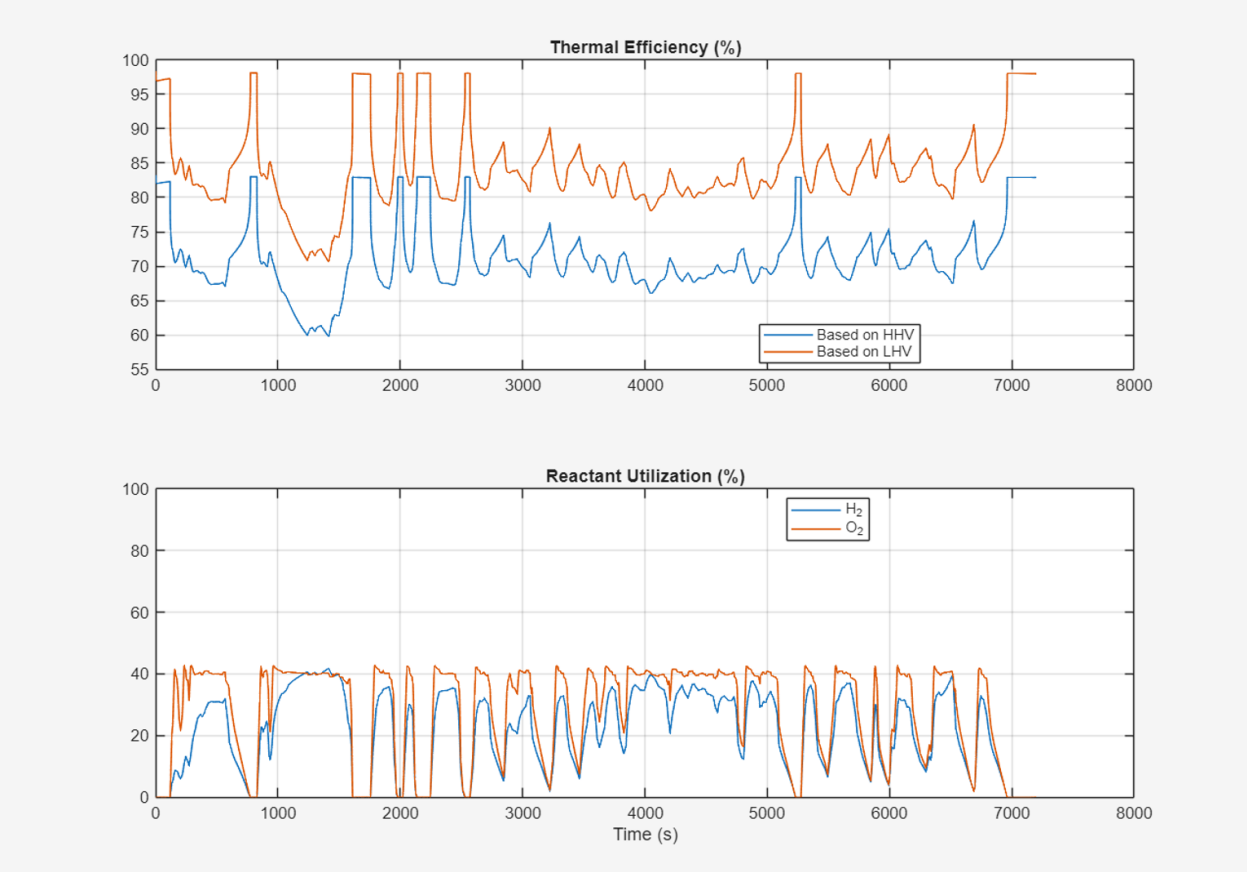

Figure 23 Fuel cell efficiency data from a fuel-cell-only run (battery commented out) using 400 cells in the stack for 7200 s, or 2 h

In the data above, the spikes in current and power indicate that the drone is consuming more power. This increased power demand could be from climbing, turning, or performing other maneuvers. The current and power graphs mirror the drone's movement. The efficiency graph shows the tradeoff: when the drone is working its hardest, the efficiency decreases. This demonstrates the strain of flight maneuvers on the propulsion system.

The next test used the same demand but half of the number of fuel cells in the stack. Using 200 cells rather than 400 would impact the system's ability to reach spikes in power demand. To avoid algebraic errors and crashes when using a smaller number of cells, a saturation block is added and connected to the drive cycle inputs. Saturation blocks allow an upper and

lower limit. For the first run using this block, the lower limit was -0.5 and the upper was 40. This means that the system would not supply more than 40 watts of power at a given moment to protect the system and prolong the simulation. This block allows a safety factor and prevents an algebraic error from overload, but it also does not reach full demand at some peaks. After confirming the successful implementation of the saturation block, simulations are run with 400 cells without saturation limits, with data recorded throughout. The battery portion of the model is added back to the simulation space in preparation for hybrid testing later in the chapter.

4.3 Battery Only Testing

Testing for the battery used a battery equivalent circuit block because this simpler block is easier to integrate within more complex systems as described below. The drive cycle block is not connected to the MEA block here because the MEA is within the fuel cell. While the previous method of commenting out the battery is satisfactory, commenting out the fuel cell with the drive cycle connected would not allow full simulation. Thus, this is a separate Simulink model with the same drive cycle connected to a circuit with a battery (Figure 24).

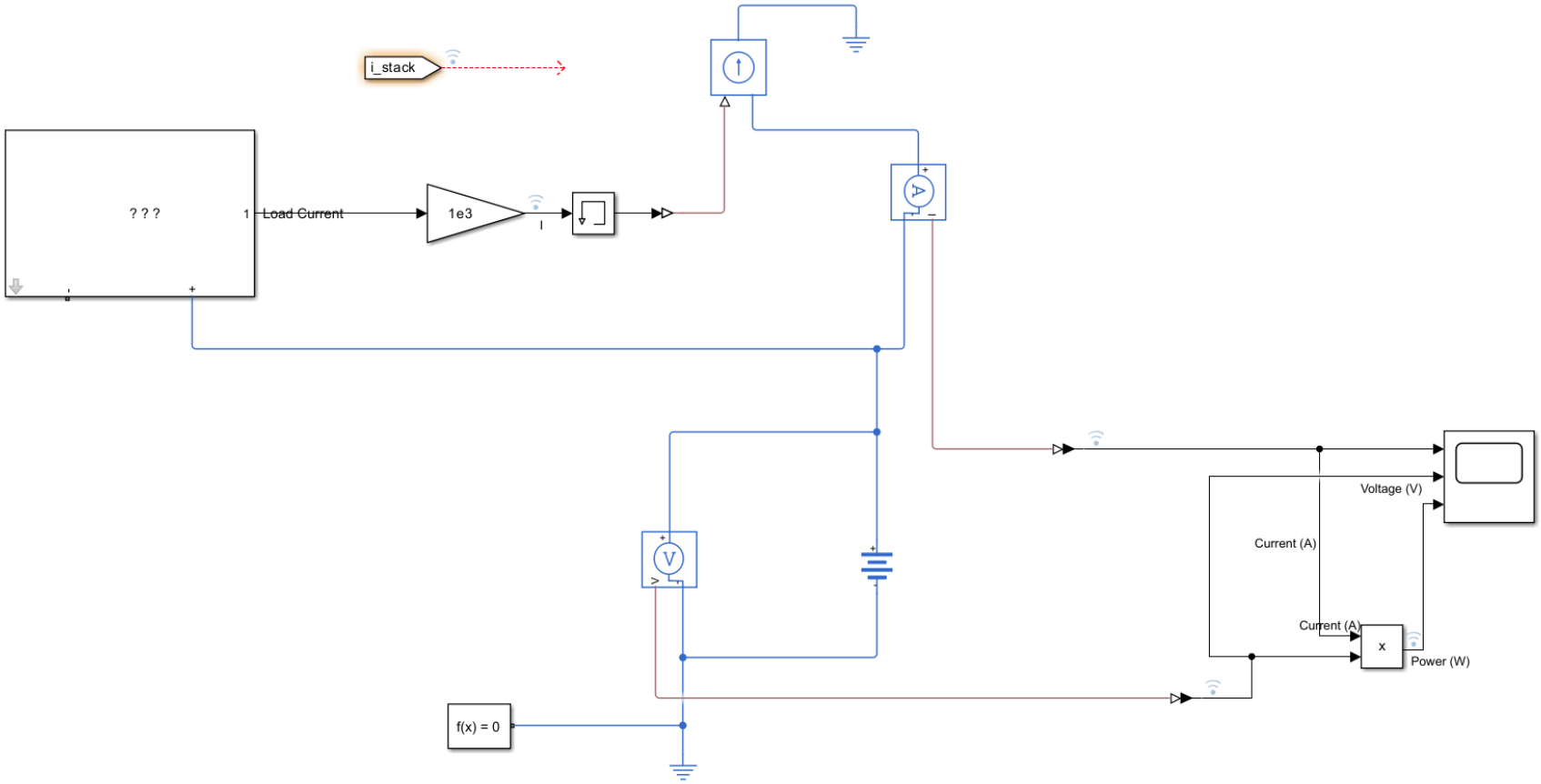

Figure 24 The battery and drive cycle, or power load, model

The left most block is the drive cycle block and supplies the power demand for the battery. The drive cycle is a more complete picture of how the battery performs with a changing power load. In contrast, a resistor is a constant load that does not have the same complexities. The triangle is a gain block that multiplies the input by one thousand to convert to the correct multiple for units. This signal travels through a controlled current source, which regulates the current. The voltage sensors, solver configuration block, signal converters, and measurement signals remain the same.

In the results below, the current and power are both recorded as negative values (Figure 25). A negative power value can signal that a component is supplying power to the rest of the system. This is the case when the battery is supplying power to meet the power demand. Another way to view this concept of negative current and power is that the battery component is a source; it is discharging throughout the simulation. If the battery is being charged or a component is consuming energy, the component is a sink, the opposite of a source.

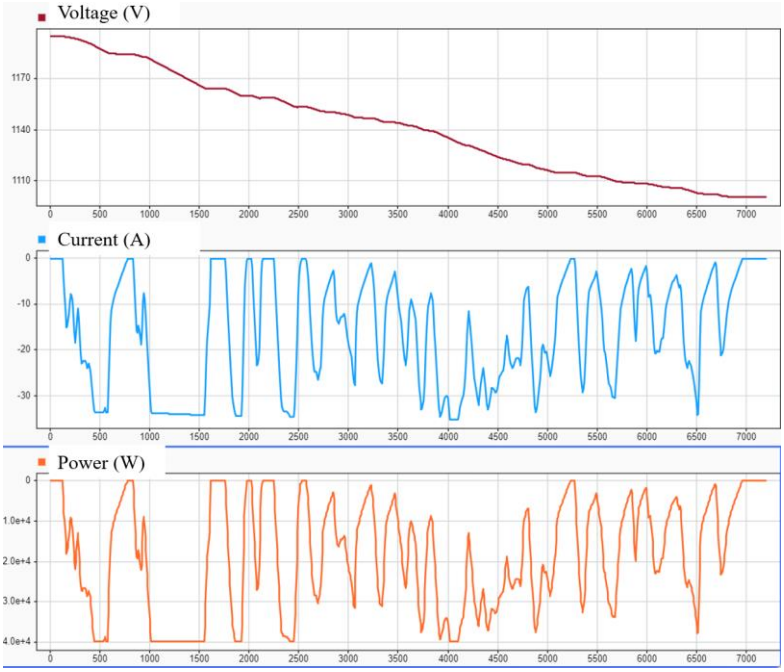

Figure 25 Data from a battery only run for 7200 s

4.4 Energy Management System

The next step in improving the model focuses on energy management systems. This system can take the drive cycle power demand and split this demand between the fuel cell and battery. One way to design an energy management system is with function blocks. A function block lets the user write a MATLAB script within the block executed as a function. The first function block in the model sees an input of the total power demand and splits this demand into two paths. The two outputs are two signals carrying half of the total power demand. These two paths each filter into two secondary function blocks. The secondary function blocks have inputs of half the power demand and the voltage from either the fuel cell or the battery for each block. The outputs of the function blocks feed into the current signals for the two power sources (Figure 26).

The MATLAB scripting method with function blocks is outside the scope of final model testing. While an energy management system is a more advanced connection strategy to control the power supplied by each method, the challenges in Simulink prevented a complete data set to compare with the rest of the results. The fuel cell–battery hybrid results are generated using a model that connects the fuel cell and battery pack by wires. An energy management system is a potential area for future work.

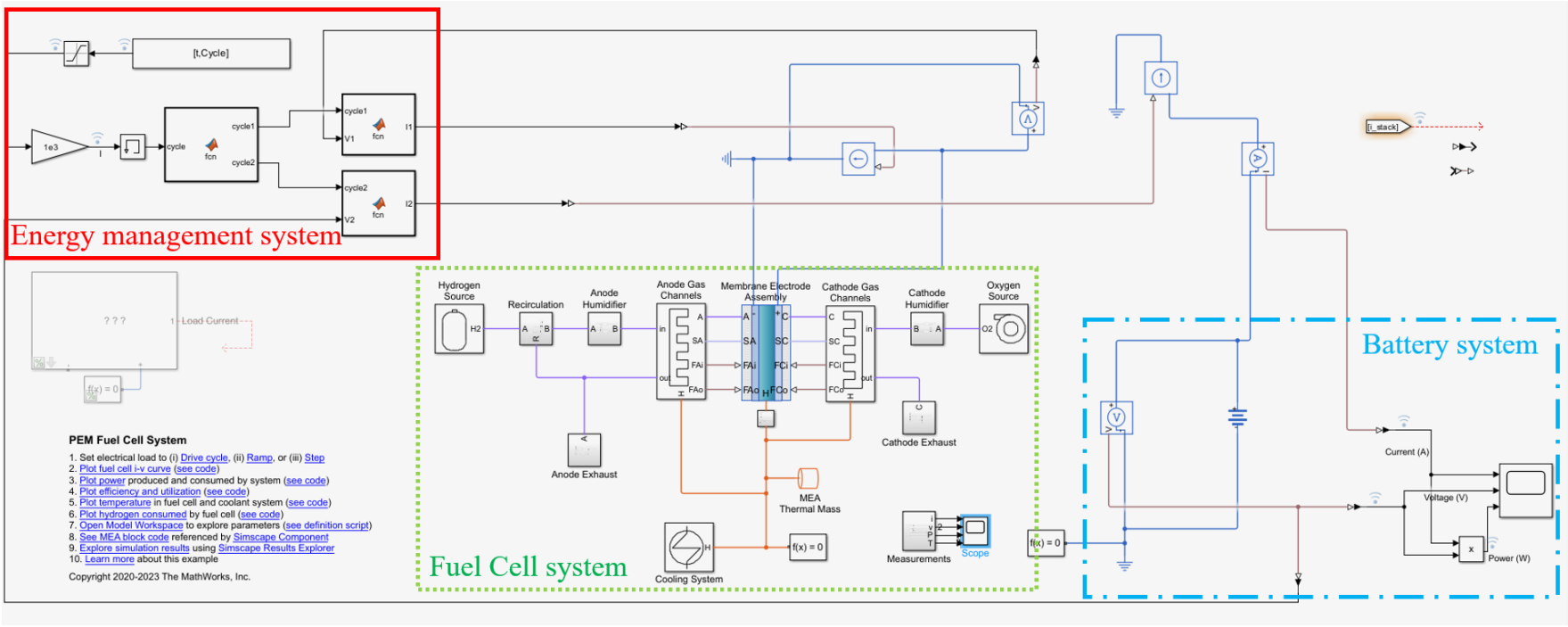

Figure 26 Function blocks model with mask on drive cycle removed, see the original block commented out, which froze at 129 s

4.5 Fuel Cell and Battery Testing

The hybrid system is connected through signal wires and includes a battery pack and a fuel cell system (Figure 27). This model is also described in chapter three and was the primary model prior to attempting to add an energy management system. This model can handle the original power demand with 400 cells for the full simulation time as seen in the graphs below (Figure 28, Figure 29, & Figure 30).

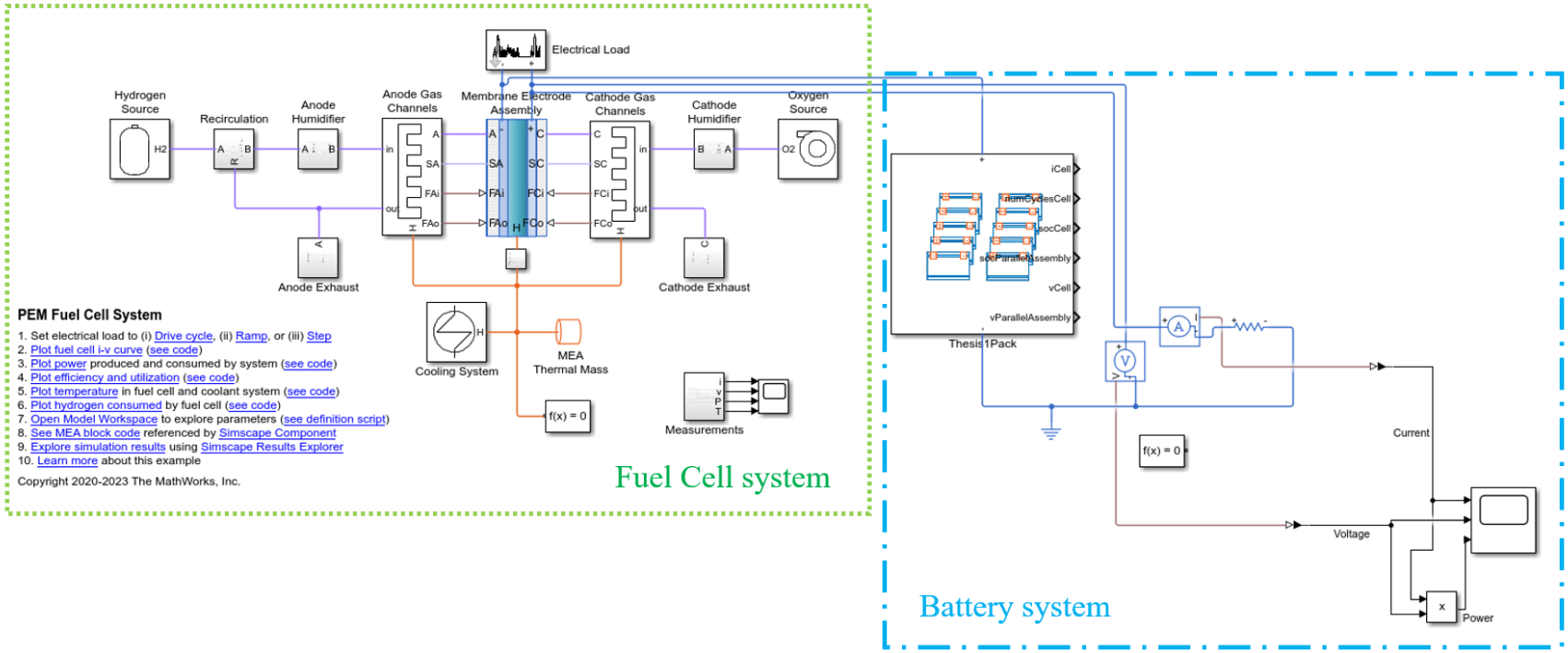

Figure 27 Model used for hybrid testing with systems connected by wires

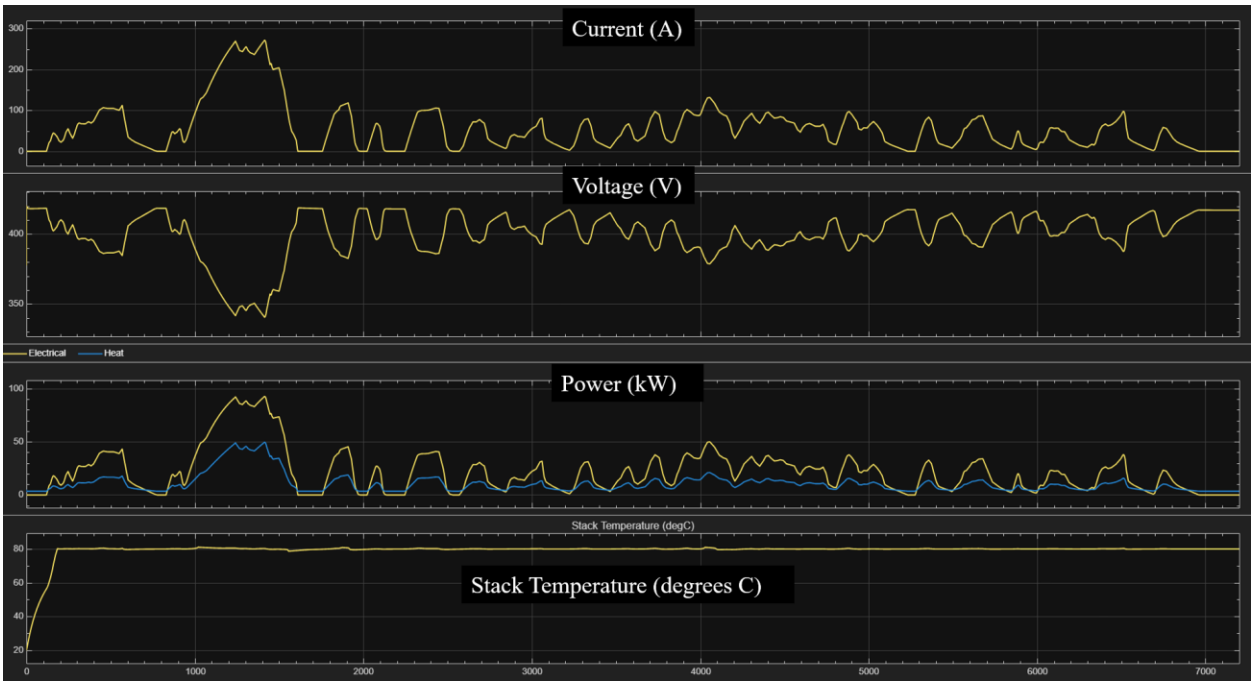

Figure 28 Fuel cell scope of hybrid run for 7200 s and 400 cells in the stack

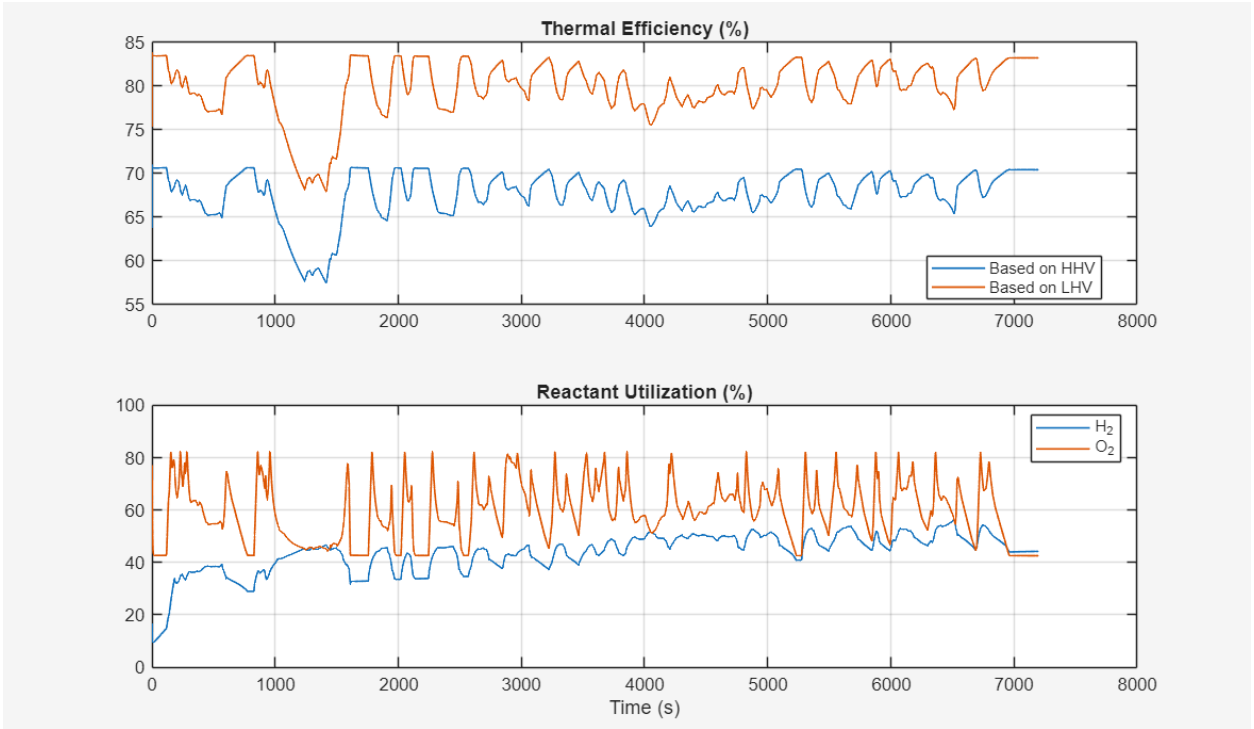

Figure 29 Efficiency from hybrid run for 7200 s with 400 cells in stack

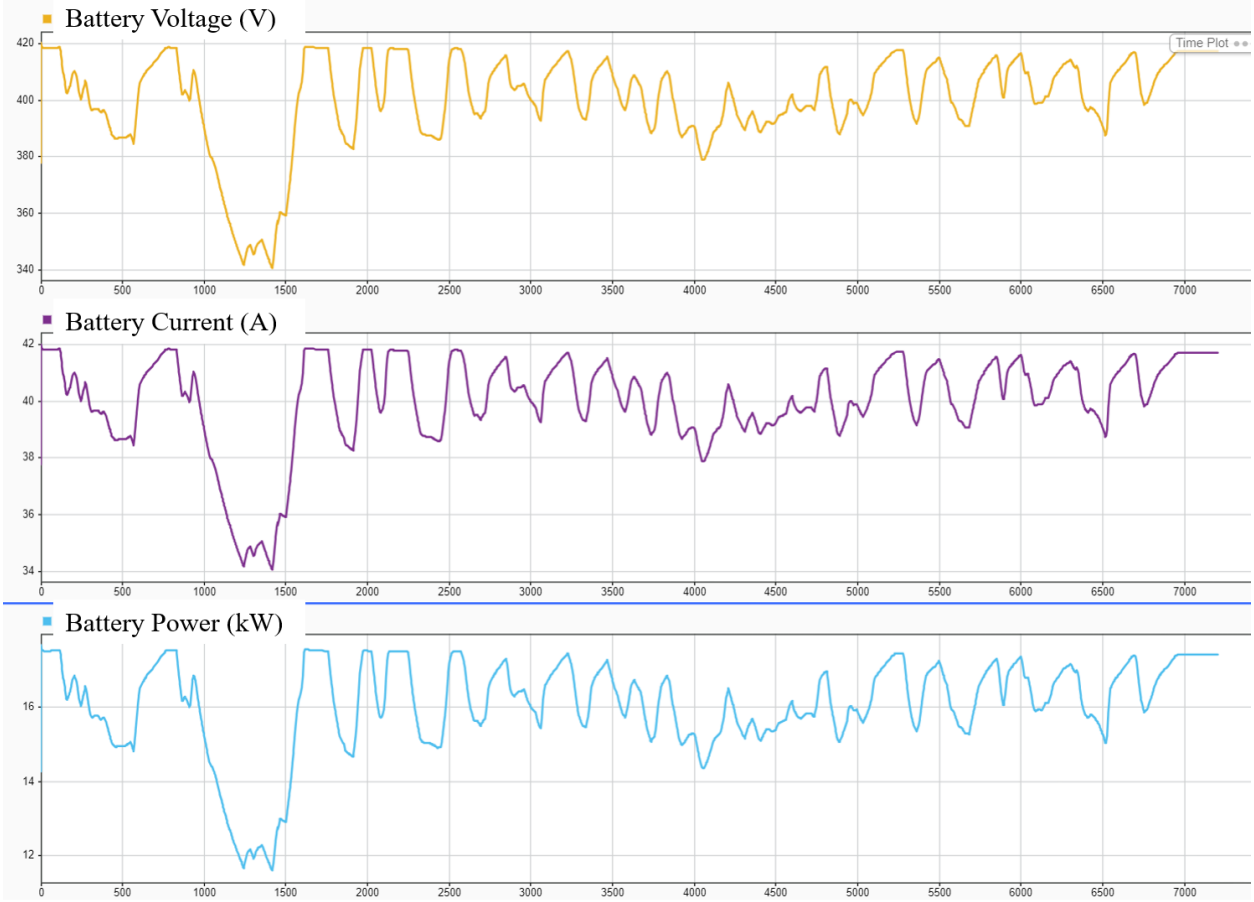

Figure 30 Battery scope of hybrid run for 7200 s and 400 cells in the stack

These graphs show the hybrid system power and endurance advantages. The battery powers sudden intense maneuvers such as takeoff, while the fuel cell powers steady cruise flight. The fuel cell avoids the high stress and failures seen in previous tests due to a battery system sharing the power load. The hybrid model uses the more powerful battery pack rather than individual battery blocks. The battery power fluctuates around sixteen kilowatts with a strong demand between one thousand and one thousand five hundred seconds. This may be attributed to the climbing phase of flight. In the same time frame, the thermal efficiency of the fuel cell drops over ten percent, indicating a high demand on the fuel cell and need for power. The power generated by the fuel cell increases in this time frame. Despite the decrease in efficiency, the fuel cell and battery are able to meet the demand of strenuous flight phases. For the remainder of the

flight, these efficiency, power, and voltage levels stabilize to average levels of oscillation. In the fuel cell only run, the efficiency of hydrogen reactant utilization fluctuated between zero to forty percent. In the hybrid runs, the hydrogen reactant efficiency peaks above fifty percent and after initial takeoff does not dip below twenty percent. This shows that a hybrid setup is more reliable for longer missions.

4.6 Parametric Study with Multiple Mission Profiles

This portion of the research replaces the original MathWorks drive cycle with three separate mission profiles. The mission profiles contain power demand values and time values up to 7,200 seconds, or two hours. The missions were generated by Gemini based on UAV weight, flight time, and flight maneuvers. The flight time given is two hours to study the UAV over a long-term mission, and the weight given is 7 kg. Each application included maneuvers such as takeoff, climb, cruise, descent, and landing. The three applications are agriculture, delivery, and surveillance. The time in seconds of each phase of the mission is listed in Table 2 below. The delivery mission has a longer descent time due to descending at the midpoint of the mission to deliver the package.

Table 2 Mission Phase Times (s)

Mission	Takeoff	Climb	Cruise	Descent	Land	Total
Agriculture	20	80	7000	50	50	7200
Delivery	20	130	6800	100	50	7200
Surveillance	20	80	7000	50	50	7200

These missions assume a constant environment. No wind resistance or extreme temperature variations are modeled, and power variations are driven by mission maneuvers. The

delivery mission assumes a hover delivery, which increases time in the climb and descent phases but does not change the takeoff or landing time compared to other missions. A loss in payload is also assumed in the delivery mission due to delivery of the package. The frame and power systems of the UAV are assumed to weigh 5 kg. The agriculture sensors and sprayer are assumed to weigh 2 kg. The delivery release mechanism is assumed to weigh 0.5 kg and the package 2 kg. The surveillance camera is assumed to weigh 1.5 kg. The cruise phases of each mission are assumed to follow a given oscillation pattern within maximum and minimum cruise values. The aerodynamic drag characteristics are assumed to be the same across missions regardless of equipment or shape of profile with added equipment.

The agriculture mission is graphed in yellow and fluctuates between forty-five to seventy-five watts throughout its cruise flight. It changes power demand consistently and with a larger range during cruise. However, the overall agriculture mission profile is constant and predictable. The package delivery mission is graphed in orange and sees the most change and fluctuation throughout cruise. The first half of the mission requires more power than the last half due to the increased payload of carrying the package prior to delivery. The large fluctuations at the halfway point may be the result of landing, delivering the package, and taking off again. These maneuvers are strenuous on the UAV; even landing can require more power than cruise in order to execute a safe and controlled landing slowly. The first half of the delivery mission is also the highest demand seen across any of the missions. The surveillance mission is graphed in blue and has the most consistency and lowest oscillation of the given missions. This relates to its real-world application of remaining at a near-constant altitude. The mission profiles are graphed in Figure 31 below.

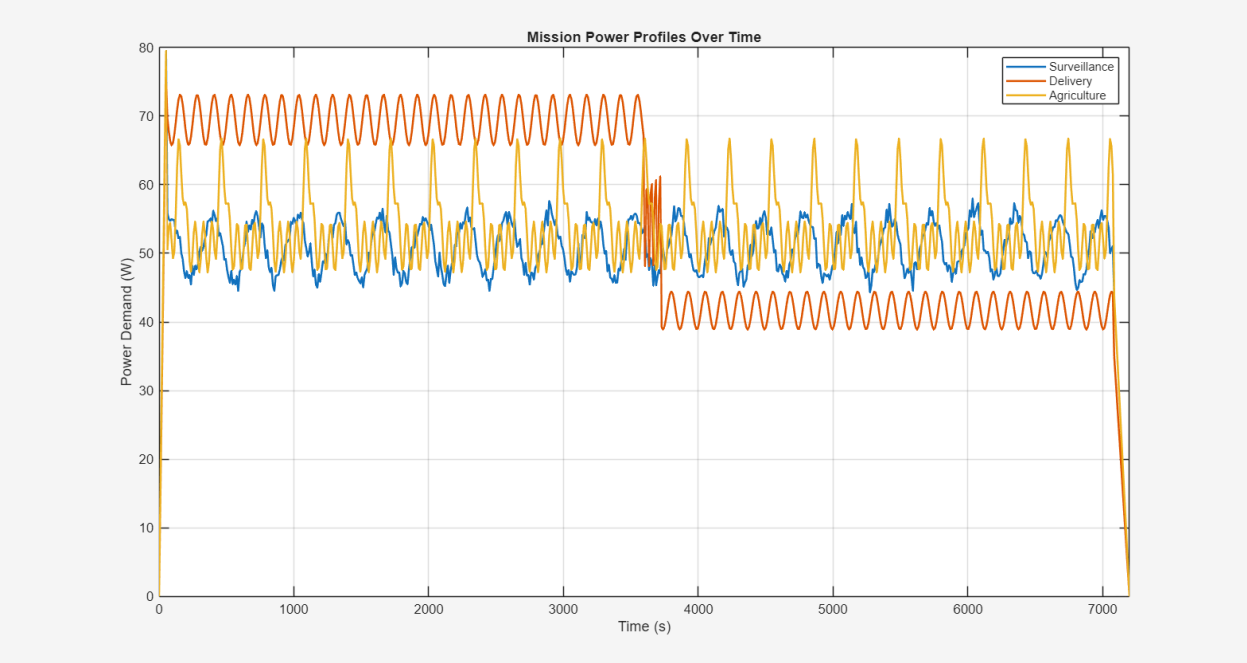

Figure 31 The three mission profiles based on real-world UAV applications

4.6.1 Agriculture Mission Profile

The initial run of the parametric study uses the agriculture mission profile (see agriculture UAV applications in chapter 2). The settings for this run are an upper saturation limit of 40 and 400 cells in the stack. The solver configuration is set to use local solver with a 0.1 s sample time. The local solver is added to these runs to implement more control over the MATLAB rate of calculations and to produce more data. This run ended at 6055.3 s. It is a fine model for an hour and a half flight mission. The results are shown in Figure 32, Figure 33, and Figure 34. The small sample time caused a prolonged simulation time compared to initial model testing. In the following two mission profiles, the sample time is adjusted to 0.5 s. These runs terminated at similar times, and the slight increase in sample time allowed a similar data scope with less time per simulation.

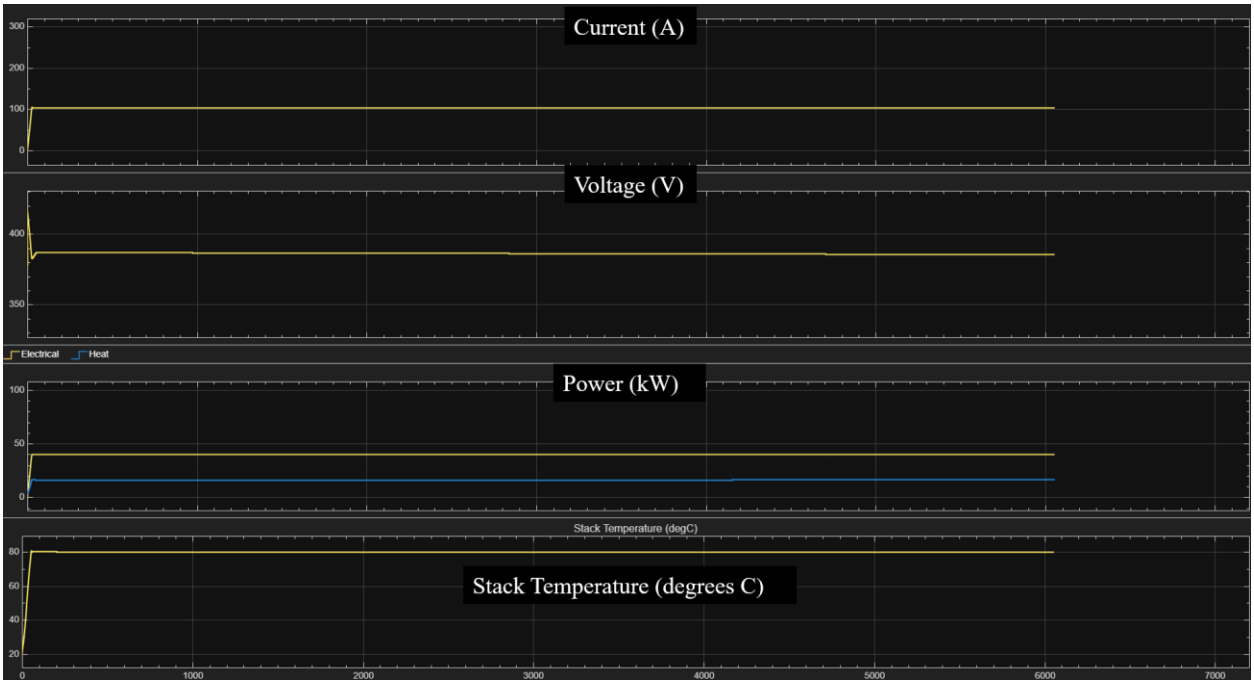

Figure 32 Fuel cell scope of agriculture mission

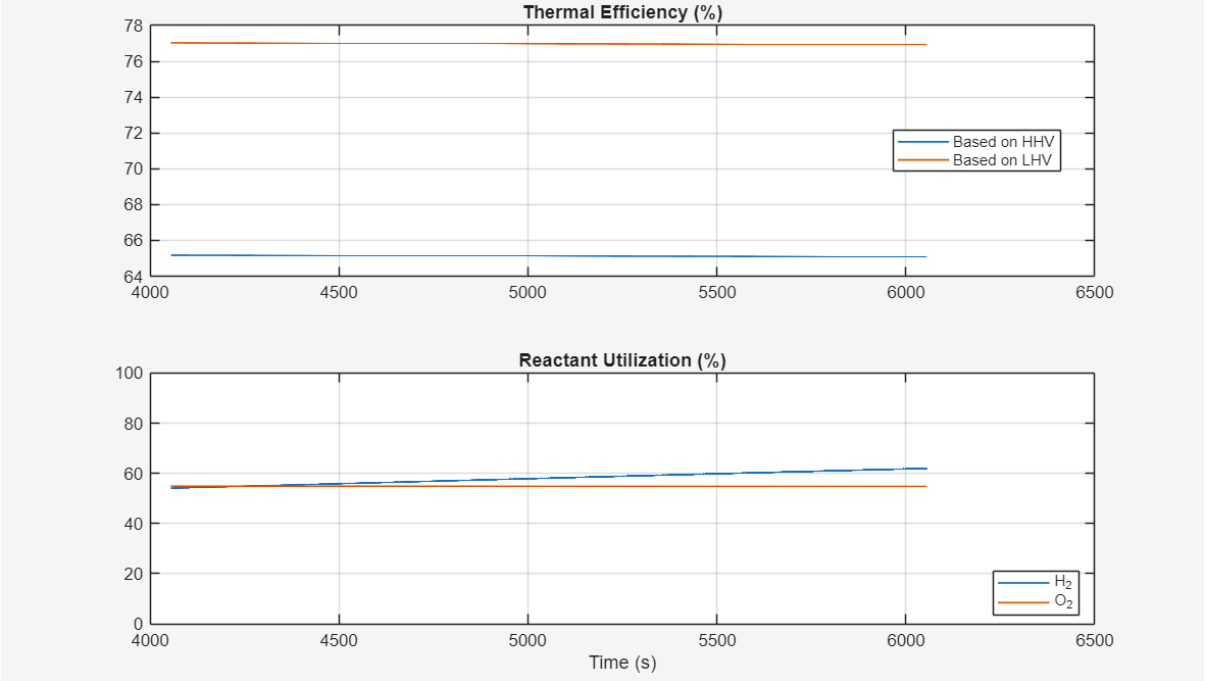

Figure 33 Fuel cell efficiency of agriculture mission

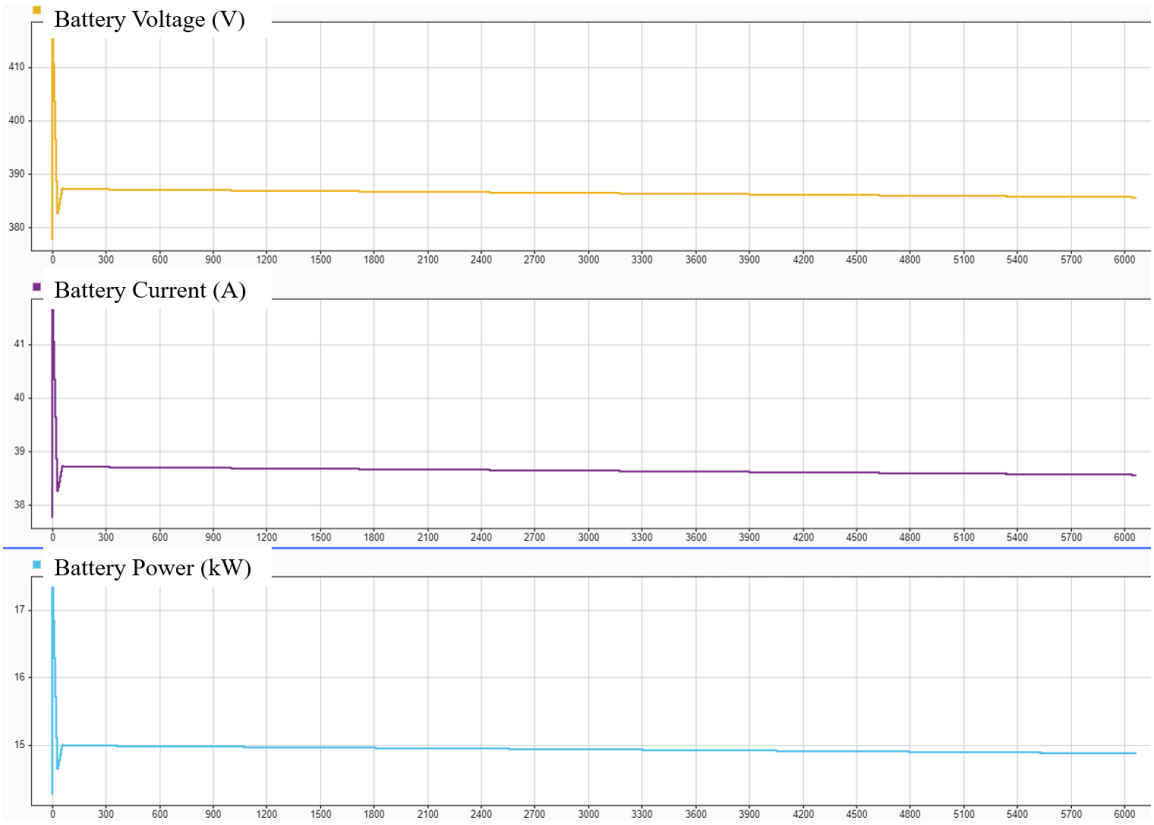

Figure 34 Battery scope of agriculture mission

4.6.2 Package Delivery Mission Profile

The second run of the parametric study uses the delivery mission profile. The settings for this run are an upper saturation limit of 40 and 400 cells in the stack. The solver configuration is set to use local solver with a 0.5 s sample time. This run ended at 4387 s and would be suitable for an hour-long mission. The results are shown in Figure 35, Figure 36, and Figure 37. The package delivery mission completed the lowest percentage of its mission in testing, which could be due to the increased power demand of additional maneuvers. The UAV must takeoff to reach the delivery site, land to deliver the package, takeoff from the delivery site, return to its home base, and finally land. This mission is unique in the landing and takeoff in the middle of the mission, and it also adds an additional payload to the UAV in carrying the package for the first half of flight. All these challenges contribute to the simulation limitations of this mission.

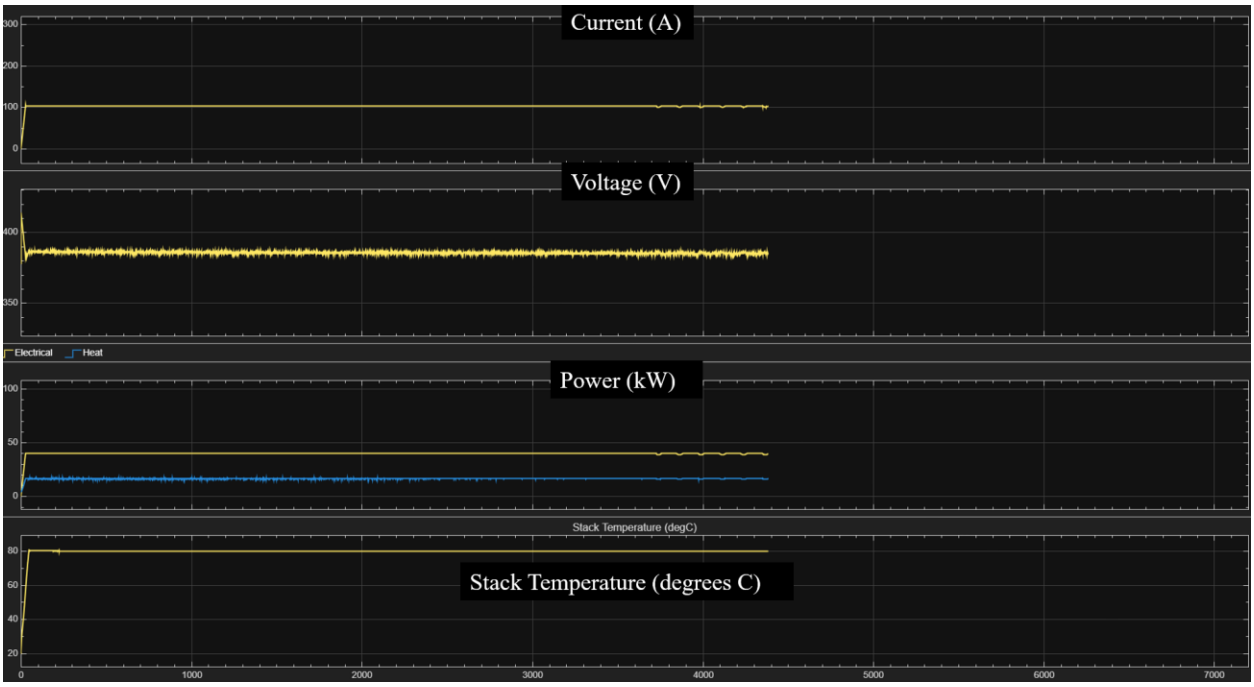

Figure 35 Fuel cell scope for delivery mission

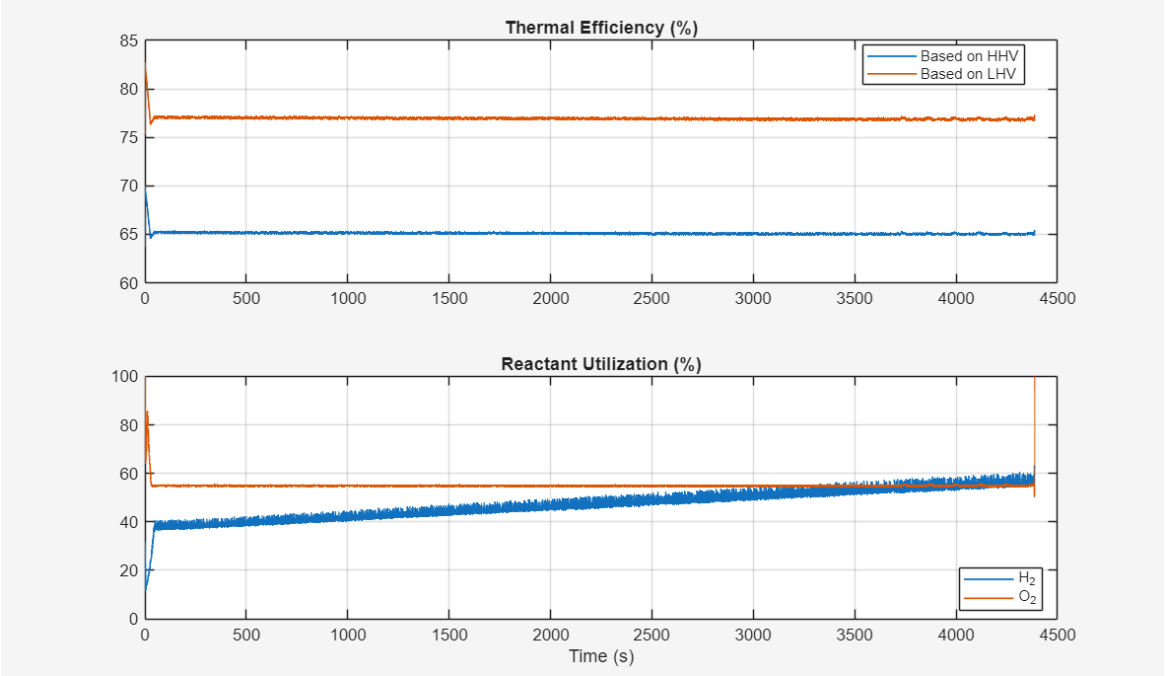

Figure 36 Fuel cell efficiency for delivery mission

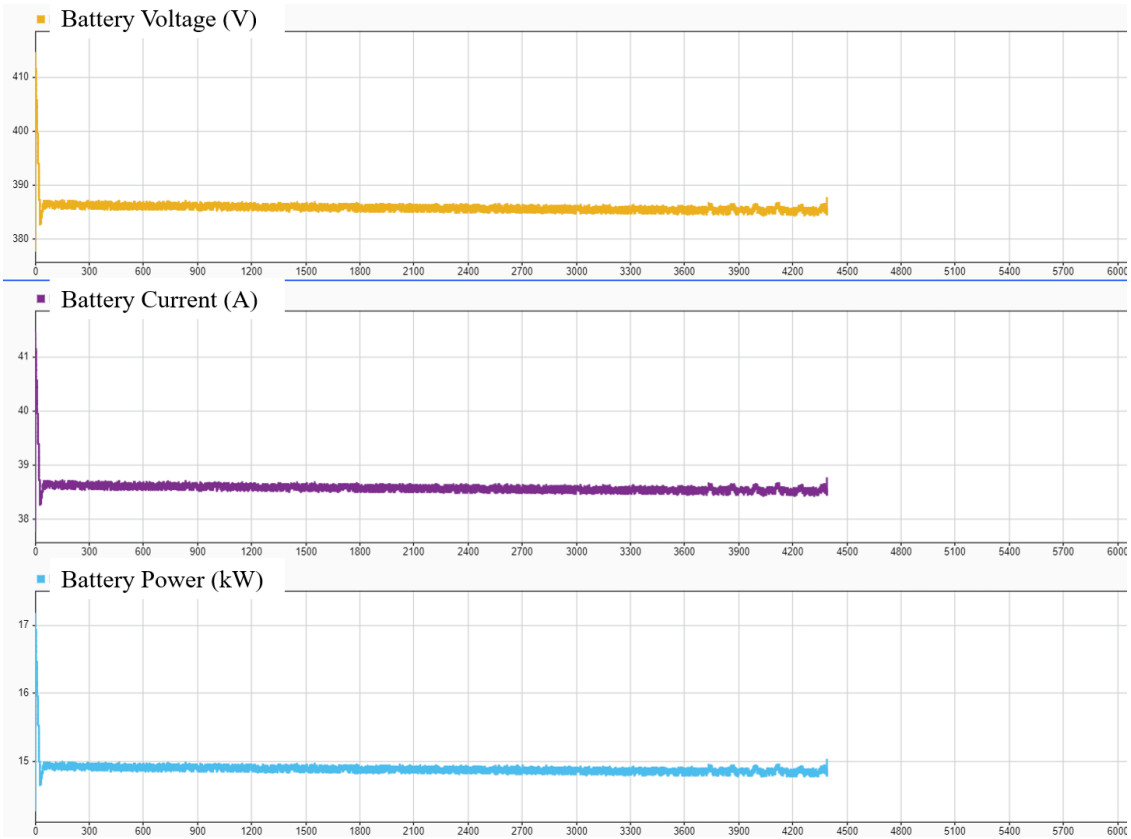

Figure 37 Battery scope for delivery mission

4.6.3 Surveillance Mission Profile

The third run of the parametric study uses the surveillance mission profile. The settings for this run are an upper saturation limit of 40 and 400 cells in the stack. The solver configuration is set to use local solver with a 0.5 s sample time. This run ended at 6057.5 s. It is a fine model for an hour and a half flight mission. The results are shown in Figure 38, Figure 39, and Figure 40. This run completes the highest percentage of its intended mission, which could be attributed to the constant power demands of the surveillance mission. In the graph showing power demand over time of all three mission profiles, the surveillance mission has two distinct advantages. It does not reach the power demand peaks of other missions, and it has the least oscillation of the three missions. In physical applications, it requires less power, and it maintains a consistent range of power, which leads to better performance.

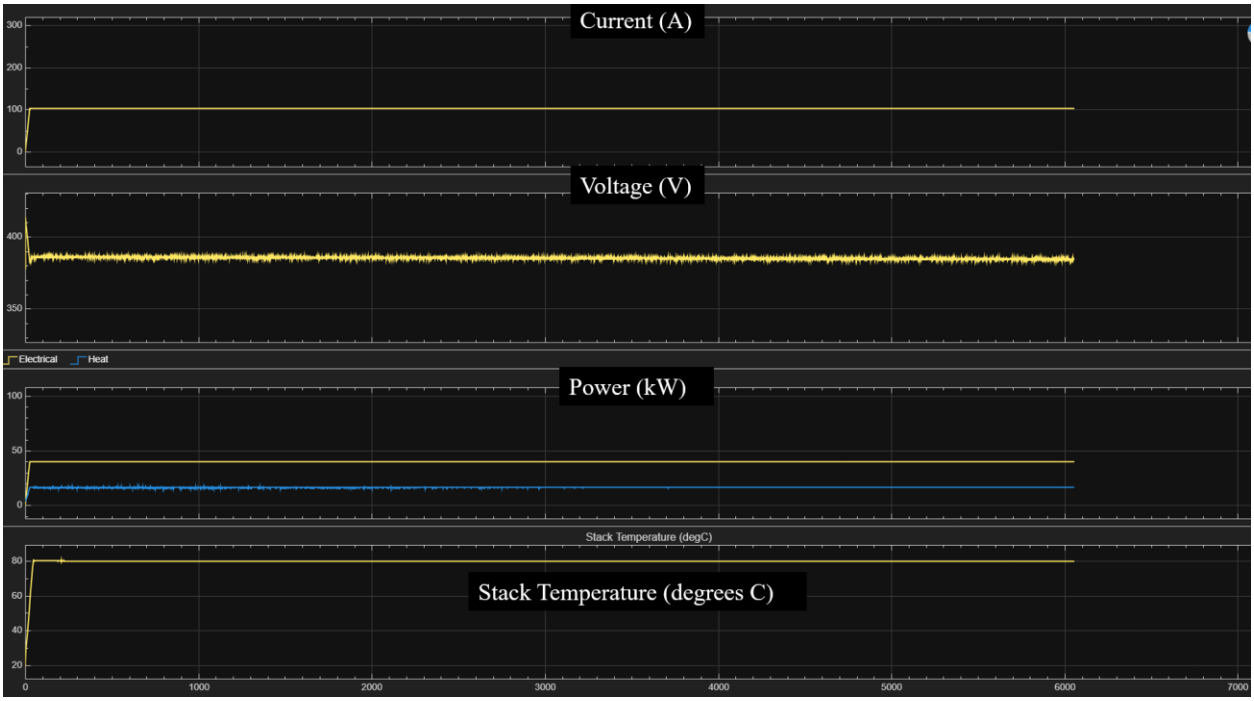

Figure 38 Fuel cell scope for surveillance mission

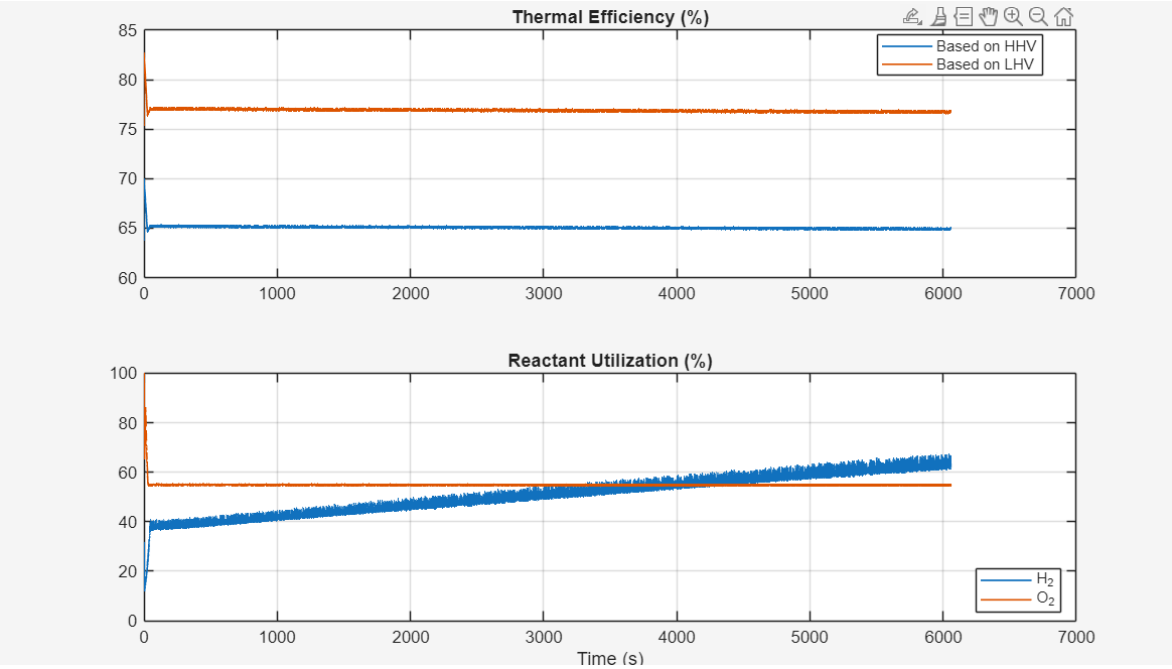

Figure 39 Fuel cell efficiency for surveillance mission

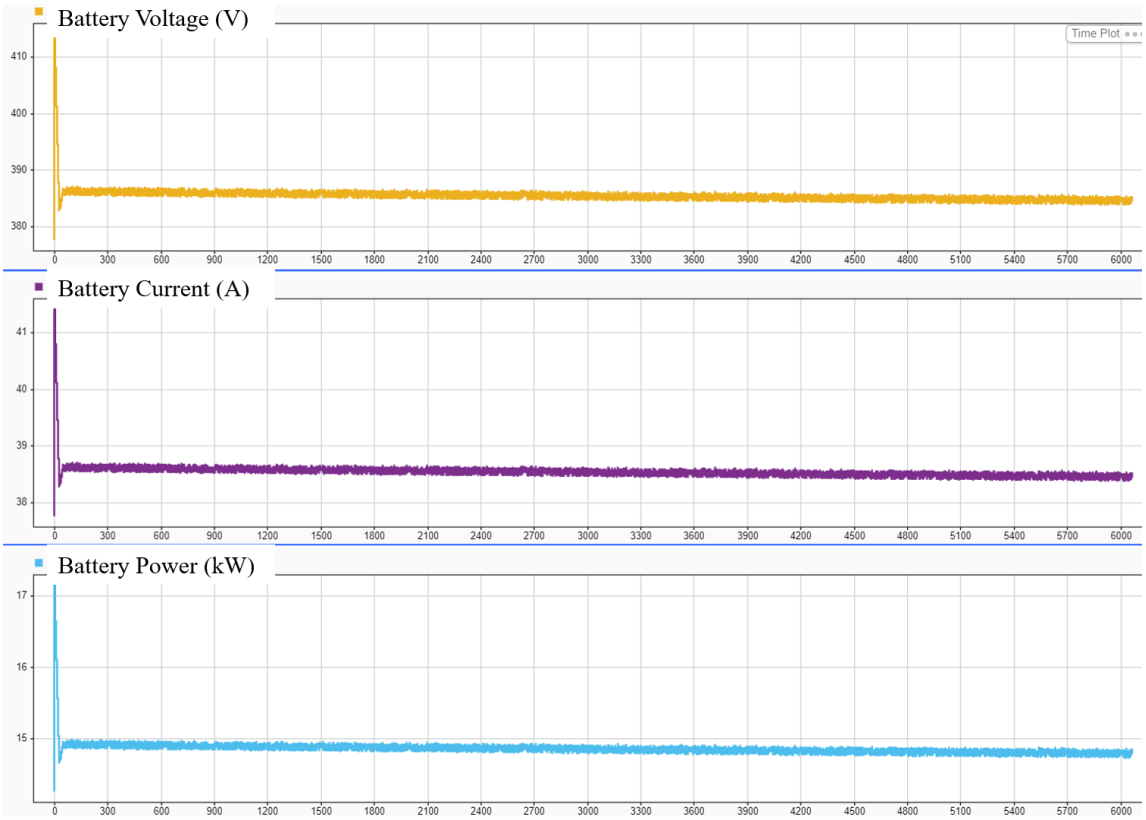

Figure 40 Battery scope for surveillance mission

4.6.4 Discussion of Results

In each of the three missions, the battery power rapidly reaches a peak and rapidly discharges, remaining low for the majority of the test runs. This signals a high power demand at takeoff and an inadequately sized battery pack. A larger battery pack may solve this problem with these missions, but for prolonged use charging the battery in-flight through the fuel cell during cruise flight would be necessary. This would require additional control systems, logic, and state of charge measurement within the model.

The efficiency of the fuel cell produced similar results in each mission, but the agriculture mission had the least oscillation in the efficiency data. The reactant utilization of hydrogen increased as the simulation continued, and the reactant utilization of oxygen remained

relatively stagnant. This could signal that the fuel cell was under more demand and consuming more hydrogen for fuel as the simulation continued.

The power in each run averages forty kilowatts during the simulation. This may be due to a saturation limit on the power, especially during the high demand for takeoff in each mission. To execute these missions for the full two hours and reach the peak power demands without simulation crash, there must be more power generated. The fuel cell system may need to be enlarged, the initial conditions may need to be modified, and the battery may need in-flight charging so that it can provide power throughout the simulation rather than exclusively at the beginning. This parametric study is a starting point for future power demands on UAVs and modeling the missions to explore necessary equipment.

Chapter 5: Summary and Future Work

5.1 Summary

This thesis explores existing UAV hybrid systems and uses this research to design and test MATLAB and Simulink models of fuel cell, battery, and hybrid systems. The fuel cell model is run with a set mission profile, and the battery model is run with the same mission profile. The hybrid model is then run to see the effects of distributing the power load across two power sources, such as less strain on the system and higher thermal efficiency. The hybrid system is simulated with three real-world applications of UAVs, and the system performance is evaluated while considering the power demand changes of each scenario. Overall, the hybrid system performs better than individual fuel cell or battery systems, and a consistent power demand can allow for longer missions and flight times.

The fuel cell system increased percentage of hydrogen reactant use over time, showing the strain on the cells and the fuel production to meet power demand as the simulation progressed. The power levels remaining at 40 kW show a system performance limited by saturation blocks for safety of the represented system. The battery power peak within the first percentage of simulation time is not adequate to power the UAV system past a short burst of power. Adjustments of battery charging, sizing, and parameters could provide a more substantial power source throughout the testing. Even for short-term missions, resizing the battery and implementing recharging could offer performance benefits.

This study explores the use of a fuel cell system and a battery system in a hybrid configuration to power a UAV. The model was adjusted to replace the original drive cycle with new drive cycles. These mission profiles tested longer mission times, various applications of UAVs, and pushed the hybrid system to its power limitations. While the test runs are better suited

to missions between 1 and 1.5 hours, this finding is vital to future research accommodating large power demands in long missions.

The use of MathWorks software was a key part of the study. Experimenting with battery packs, battery blocks, editing variables to adjust drive cycles, and writing a script to split power demand within function blocks each contributed to the research. Simulink allows a more accessible workspace than strictly MATLAB coding. A Simulink model can be shared with other researchers to easily replace mission profiles and resize power sources for unique needs. This thesis explored the MathWorks capabilities in representing and testing the system, as well as best practices to prolong the simulation and protect the proposed physical system.

5.2 Future Work Recommendations

The applications for UAVs powered by fuel cells span across industries and can vary in mission distance, flight time, altitude, and many other factors. The mission profiles and power demands presented in this thesis are a starting point for other mission applications that can be modeled and simulated through MathWorks platforms. The hybrid system can be changed as well; fuel cells can work alongside solar cells, internal combustion engines, and batteries. Future applications are not limited to only PEM fuel cells and batteries.

The models in this thesis could be externally validated in future research work. The base model of this research originates from the MathWorks library. However, the validation of the hybrid model could further support these results and allow others more information regarding the fidelity of the model. Experimental data including weather conditions, air resistance, and other factors may also impact results. Comparing these models to experiments and hardware is also an option for future work.

When connecting multiple power sources, an energy management system can be useful. The literature in chapter two discussed DC-DC converters, logic systems, and recharging the battery using energy from the fuel cell. These are all situations not modeled in this thesis, but helpful for optimizing the system and efficiency. The MATLAB function blocks in the Simulink environment tested in chapter three were used to split a load in half, and this is a fine starting point for the system. However, function blocks or converters can split power many other ways than fifty percent from each system. Depending on the size and strength of the power sources, drawing seventy-five percent of the power from one source may be the best course of action. Artificial intelligence and machine learning can also optimize a system to pinpoint the exact split between the power sources, and additional optimization through AI can improve mission success.

Individual components or code blocks were often simplified in an effort to create a model that would reach the full time of simulation and converge. Future studies could introduce more complex parts back into the model. Rather than using a Battery Equivalent Circuit block, a researcher could opt for a Battery Table Based block with more options. To achieve more power, a battery pack created in the Battery Builder MATLAB application could be the optimal choice. Battery packs have many layers to creation and more inputs and outputs to connect than a battery block. The battery pack created in this study was about 17 kW, and future researchers may want a 5- or 10-kW power supply to be able to seamlessly add battery packs in series for even more power and a scalable model.

In solver settings, the default solver method and a variable time step were selected, with the minimum and maximum time step set to auto. Creating a model that can work with smaller time steps can produce more detailed data and capture peaks or behaviors that this model would

have smoothed over. Working towards a higher fidelity model and more detailed results can give a more complete picture of the potential UAV applications.

The results of this research are promising and offer a starting point for future work. The challenges and simulation errors experienced in this research can guide future researchers in their simulation results and in predicting UAV applications for the future.

References

Adoni, W. Y. H., Lorenz, S., Fareedh, J. S., Gloaguen, R., & Bussmann, M. (2023). Investigation of autonomous multi-UAV systems for target detection in distributed environment: Current developments and open challenges. *Drones*, *7*(4), 263. https://doi.org/10.3390/drones7040263

Bayrak, Z. U., Kaya, U., & Oksuztepe, E. (2020). Investigation of PEMFC performance for cruising hybrid powered fixed-wing electric UAV in different temperatures. *International Journal of Hydrogen Energy*, *45*(11), 7036–7045. https://doi.org/10.1016/j.ijhydene.2019.12.214

Corcau, J.-I., Dinca, L., Cucu, A.-A., & Condrea, D. (2025). Drone electric propulsion system with hybrid power source. *Drones*, *9*(4), 301. https://doi.org/10.3390/drones9040301

Depcik, C., Cassady, T., Collicott, B., Burugupally, S. P., Li, X., Alam, S. S., … Hobeck, J. (2020). Comparison of lithium ion Batteries, hydrogen fueled combustion Engines, and a hydrogen fuel cell in powering a small Unmanned Aerial Vehicle. *Energy Conversion and Management., 207*. https://doi.org/10.1016/j.enconman.2020.112514

Dudek, M., Tomczyk, P., Wygonik, P., Korkosz, M., Bogusz, P., & Lis, B. (2013). Hybrid Fuel Cell – Battery System as a Main Power Unit for Small Unmanned Aerial Vehicles (UAV). *International Journal of Electrochemical Science, Volume 8* (Issue 6), Pages 8442-8463. ISSN 1452-3981.

Farajollahi, A. H., Rostami, M., & Marefati, M. (2022). A hybrid-electric propulsion system for an unmanned aerial vehicle based on proton exchange membrane fuel cell, battery, and electric motor. *Energy Sources. Part A, Recovery, Utilization, and Environmental Effects*, *44*(1), 934–950. https://doi.org/10.1080/15567036.2022.2051644

Gadalla, M., & Zafar, S. (2016). Analysis of a hydrogen fuel cell-PV power system for small

UAV. *International Journal of Hydrogen Energy*, *41*(15), 6422–6432. https://doi.org/10.1016/j.ijhydene.2016.02.129

Hartless, M. (2022, June 16). *Modeling the Protium 2500 PEM fuel cell in MATLAB Simulink*. Skydweller Aero.

Herwerth, C., Ofoma, U., Wu, C., Matsuyama, S., & Clark, S. (2006). Development of a Fuel Cell Powered UAV for Environmental Research. *AIAA Paper*, 1–14.

Hussain, I., Sibirajeshwaran, T., & Kishore, S. (2024). Rapid response drones: UAV-based healthcare delivery for critical situations. In 2024 2nd International Conference on Advances in Computation, Communication and Information Technology (ICAICCIT) (pp. 1229–1234). IEEE. https://doi.org/10.1109/ICAICCIT64383.2024.10912378

Kapoor, D. S., Singh, K. J., Bansal, R., Thakur, K., & Sharma, A. (2023). Future commercial prospects of unmanned aerial vehicles (UAVs). In S. Kumar, H. Sharma, K. Balachandran, J. H. Kim, & J. C. Bansal (Eds.), Third Congress on Intelligent Systems (pp. 79–89). Springer Nature Singapore. https://doi.org/10.1007/978-981-19-9225-4_7

Khzouz, M., Gkanas, E. I., Girella, A., Statheros, T., & Milanese, C. (2020). Sustainable hydrogen production via LiH hydrolysis for unmanned air vehicle (UAV) applications. *International Journal of Hydrogen Energy*, *45*(8), 5384–5394. https://doi.org/10.1016/j.ijhydene.2019.05.189

Kim, K., Kim, T., Lee, K., & Kwon, S. (2011). Fuel cell system with sodium borohydride as

hydrogen source for unmanned aerial vehicles. *Journal of Power Sources*, *196*(21), 9069–9075. https://doi.org/10.1016/j.jpowsour.2011.01.038

Lee, J. M., & Cho, B. H. (2009). A Dynamic Model of a PEM Fuel Cell System. *2009 Twenty-Fourth Annual IEEE Applied Power Electronics Conference and Exposition*, 720–724. IEEE. https://doi.org/10.1109/APEC.2009.4802740

Mariscal, G., Depcik, C., Chao, H., Wu, G., & Li, X. (2024). Technical and economic feasibility of applying fuel cells as the power source of unmanned aerial vehicles. *Energy Conversion and Management*, *301*, 118005. https://doi.org/10.1016/j.enconman.2023.118005

MathWorks. (n.d.). Fuel cell model: MATLAB & Simulink. Retrieved November 23, 2025, from https://www.mathworks.com/discovery/fuel-cell-model.html

Mitchell, J. W., & Braun, J. E. (2013). Combustion heating equipment (Supplemental Chapter SM 9). In *Principles of heating, ventilation, and air conditioning in buildings*. Wiley.

Ozbek, E., Yalin, G., Karaoglan, M. U., Ekici, S., Colpan, C. O., & Karakoc, T. H. (2021). Architecture design and performance analysis of a hybrid hydrogen fuel cell system for unmanned aerial vehicle. *International Journal of Hydrogen Energy*, *46*(30), 16453–16464. https://doi.org/10.1016/j.ijhydene.2020.12.216

Pan, Z. F., An, L., & Wen, C. Y. (2019). Recent advances in fuel cells based propulsion systems for unmanned aerial vehicles. *Applied Energy*, *240*, 473–485. https://doi.org/10.1016/j.apenergy.2019.02.079

PEM fuel cell system. MATLAB & Simulink. (2025). https://www.mathworks.com/help/simscape/ug/pem-fuel-cell-system.html

Pourrahmani, H., Bernier, C. M. I., & Van herle, J. (2022). The Application of Fuel-Cell and

Battery Technologies in Unmanned Aerial Vehicles (UAVs): A Dynamic Study. *Batteries (Basel)*, *8*(7), 73. https://doi.org/10.3390/batteries8070073

Samosir, A. S., Anwari, M., & Yatim, A. H. M. (2010). A simple PEM fuel cell emulator using electrical circuit model. *2010 Conference Proceedings IPEC*, 881–885. IEEE. https://doi.org/10.1109/IPECON.2010.5697090

Santos, D. F. M., Ferreira, R. B., Falcão, D. S., & Pinto, A. M. F. R. (2022). Evaluation of a fuel cell system designed for unmanned aerial vehicles. *Energy*, *253*, 124099. https://doi.org/10.1016/j.energy.2022.124099

Schlesinger, W. H., & Bernhardt, E. S. (2020). The Atmosphere. *Biogeochemistry*, 51–97. https://doi.org/10.1016/B978-0-12-814608-8.00003-7.

Toghyani, S., Atyabi, S. A., & Gao, X. (2021). Enhancing the Specific Power of a PEM Fuel Cell Powered UAV with a Novel Bean-Shaped Flow Field. *Energies*, *14*(9), 2494. https://doi.org/10.3390/en14092494

Wang, B., Zhao, D., Li, W., Wang, Z., Huang, Y., You, Y., & Becker, S. (2020). Current technologies and challenges of applying fuel cell hybrid propulsion systems in unmanned aerial vehicles. *Progress in Aerospace Sciences, Volume 116*, Pages 1-22. https://doi.org/10.1016/j.paerosci.2020.100620.

Xiao, C., Wang, B., Wang, C., & Yan, Y. (2023). Design of a novel fully-active PEMFC-Lithium battery hybrid power system based on two automatic ON/OFF switches for unmanned aerial vehicle applications. *Energy Conversion and Management*, *292*, 117417. https://doi.org/10.1016/j.enconman.2023.117417

Xu, L., Huangfu, Y., Ma, R., Xie, R., Song, Z., Zhao, D., … Xu, L. (2022). A Comprehensive

Review on Fuel Cell UAV Key Technologies: Propulsion System, Management Strategy, and Design Procedure. *IEEE Transactions on Transportation Electrification*, *8*(4), 4118–4139. https://doi.org/10.1109/TTE.2022.3195272

Yu, J., Guan, R., Li, M., Liu, Z., & Yan, J. (2021). Steady-state Simulation Analysis of Proton Exchange Membrane Fuel Cell for UAV. *International Journal of Electrochemical Science*. https://doi.org/10.20964/2021.10.30